UNIVERSITY OF CALIFORNIA MERCED

SCHOOL OF ENGINEERING

BIOLOGICAL ENGINEERING SMALL SCALE TECHNOLOGY

AIRWAY MUCUS RHEOLOGICAL PROPERTIES AND PULMONARY HEALTH

By

ERIC CHEN

A dissertation submitted in partial fulfillment of the requirements for the degree of Doctor of Philosophy at the University of California-Merced

Spring Semester, 2011

To all patients and sufferers of pulmonary diseases.

May you all be disease-free in the near future.

ACKNOWLEGEMENTS

I am greatly indebted to my advisor Prof Wei-Chun Chin for he has never failed to shed light on this dark and tortuous pathway throughout my Ph.D. years. He has provided me with a pair of insightful eyes that allows my future research to be conducted with great discernment and integrity. He has also rendered solid and vivacious platforms where I can pursue my dreams in various fields. More importantly, I have learned how to tell a great story from different perspectives. His everlasting invaluable advice and inspiration enabled me to swiftly finish my PhD with fruitful outcomes. Prof Chin was not only a fantastic advisor for my study, but also a great friend. Our friendship and his mentorship will carry on forever.

I would like to express my highest gratitude towards Profs Pedro Verdugo (University of Washington) and Paul Quinton (UCSD). A large part of my work was made possible with their mentorship. They generously provided countless hours of intellectually stimulating discussions and offered unremitting efforts to provide sign posts to guide me towards the right track. They made my Ph.D. experience even more satisfying and delightful.

I would also like to express my most sincere appreciation towards Profs David Ojcius and Linda Hirst for serving as my thesis committee members. They gave me precious encouragements, suggestions and critiques. I am especially grateful for Prof David Ojcius's arrangement to present my work at CGU. I thoroughly enjoyed the stimulating experience.

I would like to thank all my former and current undergraduate students (Andrew Wang, Maria Garnica, David Daley, Alan Richard, Alex Mintz, David Lu, Albert Sun, Miguel Ruvalcaba, Lindsey Araujo, Ryan Chapman and Joe Lee) for helping out with the experiments throughout the last 5 years. It has been a great pleasure working with you and learning from all of you. Your laughter, hard work and personalities made this lab a wonderful home for all of us.

I would like to further express my sincere thanks to friends at UC Merced who have offered endless helps. In particular, Chi-Shuo Chen, a brilliant colleague, an outstanding graduate student and a dedicated friend, who has bestowed upon me many lectures on lithography techniques. Chi-Shuo has also generously contributed toward many publications and my understanding in Bio-MEMs and fabrication in general. Our lifelong friendship will carry on both professionally and personally.

Lastly, I deeply appreciate my wife and family members who gave my everlasting support when I needed them the most. Especially my wife, she has been halting her career development for the last 2 years just to take great care of me. My Ph.D. experience was forever more pleasurable because of her accompany.

TABLE OF CONTENTS

ABSTRACT

Airway mucus gel plays a vital role in maintaining the integrity of mucosal epithelia and protecting respiratory health. Such defensive mechanism stems primarily from a constant clearance of mucus-entrapped inhaled pathogens and particulates by mucociliary transport. The success in removing mucus-entrapped harmful substances relies heavily on proper mucus rheology. It is well established that hydration is the single most important determinant of mucus rheological properties. In a healthy condition, the body precisely controls the degree of mucus hydration through modulating physiological parameters of various ionic concentrations in the nascent microenvironment which bathe the mucus. On the contrary, inadequate mucus hydration and abnormal mucus hypersecretion seem to be the major causal factors underlying pathological states involving the accumulation of highly viscous mucus plugs, obstructive airflow, chronic infection and inflammation. These symptoms are characteristic of pulmonary diseases including, but not limited to, chronic obstructive pulmonary disease (COPD), asthma, and cystic fibrosis (CF).

My research focused on the mechanisms of how (i) environmental and (ii) physiological factors affect mucus secretion and rheological properties. My first project tested whether titanium dioxide nanoparticles (TiO_2 NPs), a common air pollutant that constitutes airborne particulate matter, can induce mucin hypersecretion from airway epithelial cells via a Ca^{2+}-mediated pathway. Aside from being an airborne pollutant, many engineered NPs are utilized in the nanoindustry and have acquired secondary surface modifications. The question of functionalized NPs with surface charges being able to alter mucus rheological properties is the focal point of the second project. The third study aimed at understanding how physiological parameters involving bicarbonate ion concentrations regulate mucus rheological characteristics. Abnormal bicarbonate levels in humans have recently been suggested to instigate a devastating Caucasian disease, cystic fibrosis.

A more in-depth comprehension of how both environmental and physiological factors disturb mucus rheology and over-secretion facilitate the design of future therapies to counteract the concomitant pathologies.

CHAPTER 1

Introduction

Airway mucus plays an essential role in maintaining mucosal moisture and protecting respiratory health. The defensive mechanism derives mainly from a concerted orchestration of mucociliary transport where inhaled pathogens and particulates are constantly cleared. Mucins are large, highly glycosylated proteins consisting of an array of mucin peptides (apomucin) [1,2]. To date, 20 different mucin proteins (MUCs) are known to exist in humans, with MUC5AC and MUC5B being the predominant airway-associated mucins. MUC5AC is constitutively produced by surface goblet cells of proximal airway whereas MUC5B is generated by surface secretory cells throughout the airway and by submucosal glands [3,4,5,6,7]. Airway mucins are in a gel form which contains properties of an elastic solid and a viscous fluid [4,8,9,10]. In healthy conditions, mucus is comprised of approximately 3% solid (mucins and other proteins) and 97% water [3,4,8,9,10,11]. The high molecular weight of mucin glycoproteins is composed of ~75% carbohydrate and ~25% protein [2,3]. Rich carbohydrates provide terminal sugars with sulfate, and carboxyl (COO^-) groups rendering mucin with a polyanionic nature [2,3,6]. Complementing mucin anionic features, cationic calcium ions can act as crosslinkers that condense the mucin matrices inside secretory granules before exocytosis [2]. Upon release, phase transition mainly driven by the Donnan effect triggers the massive decondensation of mucin networks [2]. Physical entanglement, hydrogen bonding, hydrophilic and hydrophobic interactions have also been shown to contribute to the gel properties of mucin [2]. More importantly, the rheological properties of mucin gel are critical for maintaining the integrity of epithelial mucosa by trapping bacteria and viruses for mucociliary clearance. Deviation from the normal rheological properties most invariably results in pathological consequences in the pulmonary system [2,3,6,12,13,14].

Hydration is the single most important determinant of mucus rheological properties. Improper mucus hydration and mucus hypersecretion seem to be the reasons underlying the pathological obstructive mucus and impaired mucociliary transport. As a result, the

dehydrated and highly viscous mucus plugs that accumulate in airway passages and limit airflow are commonly observed throughout pulmonary diseases including chronic obstructive pulmonary disease (COPD), asthma, and cystic fibrosis (CF) [15,16]. Subsequent sequelae of mucus obstruction may accompany chronic bacterial infection, inflammation and airway remodeling [16,17]. Therefore, a delicate balance between (i) secretion and (ii) viscoelasticity are clearly indispensable to preserving pulmonary homeostasis. Interplay of these two parameters with physiological and environmental factors thus, becomes the area of interest in my study.

Under physiological condition, mucin secretion is closely regulated by cytosolic Ca^{2+} concentrations ($[Ca^{2+}]_C$) in various epithelial cells [18]. A rise in $[Ca^{2+}]_C$ initiates a cascade of down stream events including the mobilization of granule-bound Ca^{2+}, docking of the secretory granules, fusion of the plasma-granule membrane and the formation of secretory pores, therefore leading to the exocytosis of the mucin granules [19]. However, abnormal elevation of intracellular Ca^{2+} levels due to environmental factors may lead to mucus hypersecretion, potentially resulting in obstructive mucus accumulation and impaired mucociliary clearance. Pollution associated airborne particulates have been the major harmful stimulants that predispose to pulmonary morbidity and mortality. It is widely demonstrated that nanoparticle (NP) exposure through ambience and/or work place poses great threats to pulmonary wellbeing. Inhalation of NPs aggravates clinical manifestation of patients with existing respiratory symptoms. Recently, an epidemiological link between environmental NP exposure and mucus hypersecretion has been suggested. However, whether NPs can directly induce mucus hypersecretion is not clear and the mechanism behind the hypersecretory response remains elusive. It is therefore my interest to investigate whether titanium dioxide NPs can directly trigger mucin secretion from airway epithelial cells via an intracellular Ca^{2+} signaling mediated pathway.

Beside mucin secretion, altered viscoelastic properties of mucus can lead to concomitant pathological outcomes. Traditional studies examined nanotoxicity on pulmonary systems by investigating airway epithelial cell apoptosis. NPs with varying sizes and compositions were tested for their cytotoxic effects and related mechanisms. Recently,

due to advancements in nanotechnology, attention has been focused on the NP surface functionalization. Whether NP surface modifications can directly impinge harmful consequence on the viscoelastic properties of mucus has never been studied. My second project focuses on how positively-charged functionalized NPs impede mucus hydration.
Apart from environmental factors, physiological parameters also modulate rheological properties of mucus. The long standing cationic paradigm has shown profound impact on viscoelastic properties of gel-forming mucin. However, possible contribution from anions in mucus formation and the lack of which can cause impaired mucus rheology has received little attention. Hence, my last study examines the effects of bicarbonate anions on mucin rheological characteristics.

My Ph.D. thesis provided a more in-depth understanding of how both environmental and physiological factors influence mucin secretion and rheological properties. Through these projects, I aim to help provide future therapeutic treatments to restore mucin homeostasis and ameliorate symptoms of pulmonary diseases.

CHAPTER 2

Mucin Secretion Induced by Titanium Dioxide Nanoparticles

ABSTRACT

Nanoparticle (NP) exposure has been closely associated with the exacerbation and pathophysiology of many respiratory diseases such as Chronic Obstructive Pulmonary Disease (COPD) and asthma. Mucus hypersecretion and accumulation in the airway are major clinical manifestations commonly found in these diseases. Among a broad spectrum of NPs, titanium dioxide (TiO_2), one of the PM10 components, is widely utilized in the nanoindustry for manufacturing and processing of various commercial products. Although TiO_2 NPs have been shown to induce cellular nanotoxicity and emphysema-like symptoms, whether TiO_2 NPs can directly induce mucus secretion from airway cells is currently unknown. Herein, we showed that TiO_2 NPs (< 75 nm) can directly stimulate mucin secretion from human bronchial ChaGo-K1 epithelial cells via a Ca^{2+} signaling mediated pathway. The amount of mucin secreted was quantified with enzyme-linked lectin assay (ELLA). The corresponding changes in cytosolic Ca^{2+} concentration were monitored with Rhod-2, a fluorescent Ca^{2+} dye. We found that TiO_2 NP-evoked mucin secretion was a function of increasing intracellular Ca^{2+} concentration resulting from an extracellular Ca^{2+} influx via membrane Ca^{2+} channels and cytosolic ER Ca^{2+} release. The calcium-induced calcium release (CICR) mechanism played a major role in further amplifying the intracellular Ca^{2+} signal and in sustaining a cytosolic Ca^{2+} increase. This study provides a potential mechanistic link between airborne NPs and the pathoetiology of pulmonary diseases involving mucus hypersecretion.

Keyword: Titanium dioxide nanoparticle, nanoparticles, mucin secretion, intracellular calcium signaling, exocytosis, airway cells

INTRODUCTION

Many published reports have demonstrated the association between NP exposure and pulmonary morbidity and mortality [20,21,22]. The adverse effects induced by NPs seem to exacerbate clinical symptoms of pre-existing respiratory illnesses such as asthma, COPD and Cystic Fibrosis (CF) [20,21,22,23,24,25]. During NP exposure, individuals with respiratory diseases showed more incidences of bronchoconstriction, medication use, bronchial hyperreactivity and lung fibrosis [21,26]. TiO_2 NPs are widely used in the nanotechnology industry due to their vast array of applications that range from household commodities, such as components of paints and carpets, to personal products that include cosmetics, textiles, sunscreens and foods [27,28]. TiO_2 is also one of the PM10 components commonly found in industries or manufacturing plants involved in processing mineral ore rutile [29]. It has been reported that > 50% of TiO_2 NP exposed workers had respiratory symptoms accompanied by reduction in pulmonary function [29,30]. Other reports have also indicated that inhalation of TiO_2 NPs can induce pulmonary inflammatory responses (characterized by neutrophil recruitment), epithelial cell death and increased permeability [21,28]. Furthermore, TiO_2 NPs have been shown to play a role in inducing epithelial fibroproliferative changes, stimulating goblet cell hyperplasia and in instigating emphysema-like (such as alveolar enlargement) damages in the lungs [21,29,31]. Overall, nanotoxicity induced by TiO_2 NP exposure in both the occupational and ambient environment presents a significant and realistic health concern.

The harmful effects of NPs on the respiratory system not only encompass cellular apoptosis/necrosis, but also mucus hyperproduction which is closely associated with the pathogenesis of pulmonary diseases that include asthma, COPD and CF [21,29,32]. In these chronic pulmonary diseases, mucus hypersecretion and accumulation may lead to recurrent episodes of chronic bacterial infections, limited airflow and chronic inflammatory responses [21,33,34]. However, whether TiO_2 NPs can directly induce mucin secretion has not been resolved.

Airway mucus plays a vital role in the constant clearance of inhaled pathogens and particulates. Mucus is a large, highly glycosylated protein consisting of an array of mucin

peptides (apomucin) [33]. With their oligosaccharide sidegroups, such as sialic acid, sulfate, and carboxyl (COO^-), mucins are usually polyanionic in nature [2]. Mucin secretion is closely regulated by cytosolic Ca^{2+} concentrations ($[Ca^{2+}]_C$) in various epithelial cells [18]. A rise in $[Ca^{2+}]_C$ is crucial for initiating a cascade of down stream events including the mobilization of granule-bound Ca^{2+}, docking of the secretory granules, fusion of the plasma-granule membrane and the formation of secretory pores, therefore leading to the exocytosis of the mucin granules [19].

Agonist-induced opening of various Ca^{2+} channels expressed on the cell membrane allows the influx of extracellular Ca^{2+}, which may serve as the external Ca^{2+} source [35]. The initial upsurge in the $[Ca^{2+}]_C$ is usually relayed by triggering a secondary wave of Ca^{2+} propagation from internal stores, such as the ER [35,36,37,38]. Ryanodine receptors (RYRs) on the ER have multiple allosteric Ca^{2+} binding sites responsible for triggering Ca^{2+}- induced Ca^{2+} release (CICR) into the cytosol [35,36,37,38]. The resultant increase in $[Ca^{2+}]_C$ could activate other cytosolic proteins and modulate secretion of mucin, hormones or various neurotransmitters [18,39,40].

NPs have been shown to disturb cellular functions by elevating intracellular Ca^{2+} levels [41,42,43,44]. For example, ultrafine carbon black NPs can elicit Ca^{2+}-dependent secretion through the activation of L-type voltage-gated Ca^{2+} channels [41,42,44]. However, little is known regarding the intricate calcium signaling pathway regulating the exocytotic events of secretory products. In this study, we aim to investigate the mechanism through which TiO_2 NPs induce mucin secretion via a Ca^{2+} signaling mediated pathway.

MATERIALS AND METHODS

1. Culture of ChaGo-K1 cells

The human airway bronchial epithelial cell line ChaGo-K1, obtained from American Type Culture Collection (ATCC, Manassas, VA, USA), was used because it expresses MUC proteins and secretes mucin [45]. Cells were cultured in 15 cm cell culture plates (VWR, CA, USA) in RPMI 1640 medium (Invitrogen, CA, USA) supplemented with L-glutamine, 1% penicillin/streptomycin and 10% heat inactivated fetal bovine serum (FBS). Cultures were incubated in a humidified incubator at 37℃/5% CO_2. Cell counts were performed using trypan blue (Sigma-Aldrich, MO, USA) exclusion and a Bright-Line haemocytometer.

2. Nanoparticles and characterization

A mixture of anatase and rutile forms of ultrafine titanium (IV) dioxide (< 75 nm) (Sigma-Aldrich, MO, USA) was used in this study because this form has been shown to result in more severe cellular injuries [46,47]. The TiO_2 NPs have a surface area of 36 m^2/g and the dispersion conductivity is 1040 μS/cm (information from Sigma). All NP samples were sonicated before usage. The concentrations used were 1 mg/ml, 0.75 mg/ml, 0.5 mg/ml, 0.25 mg/ml, 0.1 mg/ml, and 0.05 mg/ml. The range of concentrations used was consistent with the concentrations of TiO_2 NPs found in previous reports [46]. The TiO_2 NPs were reconstituted with Hanks' solution (Invitrogen, CA, USA) before being tested. The size of NPs was independently confirmed using homodyne dynamics laser scattering (DLS) as described in previous studies [13,14].

3. Cell preparation

Cells were seeded at 2×10^5 cells per well in a 24-well plate, and incubated for 24 hrs in RPMI 1640 supplemented with 10% FBS. Following 24 hr incubation, the RPMI medium was removed from the cells and the culture was rinsed with Hanks' solution twice before use.

4. Measurements of cytosolic Ca^{2+} concentrations induced by TiO_2 exposure

The cells were then loaded with a Rhod-2 AM dye (1 μM) (K_d = 570 nM, λ_{Ex} = 552 nm and λ_{Em} = 581) (Invitrogen, CA, USA) for 45 minutes. After the dye loading, the cells were rinsed, incubated with either normal Hanks' or Ca^{2+}-free Hanks' solution, and treated with the appropriate TiO_2 concentrations. All calcium signaling experiments were carried out on a thermoregulated stage at 37℃ mounted on a Nikon microscope (Nikon Eclipse TE2000-U, Tokyo, Japan). ChaGo-K1 cells were incubated with cadmium chloride (200 μM; Sigma-Aldrich, MO, USA) to block the membrane Ca^{2+} channels [48], followed by TiO_2 NP stimulation. To investigate the interaction between TiO_2 and membrane Ca^{2+} channels, nifedipine (10 μM; Sigma-Aldrich, MO, USA), an L-type Ca^{2+} channel blocker [43], was added to ChaGo-K1 cells prior to the exposure of TiO_2. Antioxidant N-acetylcysteine (NAC, 250 μM; Sigma-Aldrich, MO, USA) was also added to ChaGo-K1 cells to study the involvement of reactive oxygen species (ROS) [43,49], possibly generated as a result of TiO_2 stimulation, and the activation of Ca^{2+} channels. Thapsigargin (100 nM; Sigma-Aldrich, MO, USA) [19] and ryanodine (100 μM; Sigma-Aldrich, MO, USA) were added separately to deplete the ER Ca^{2+} content and to inhibit the CICR mechanism [36,37], correspondingly. These two blockers were utilized to investigate the contribution from the internal ER Ca^{2+} pool.

5. Calcein dye leakage measurements

ChaGo-K1 cells were seeded at the density of 2×10^5 cells per well in a 24-well plate and cultured for 24 hrs. TiO_2 NP prepared with calcein fluorescent dye (50 μM) (Invitrogen, CA, USA) in Hanks' solution was incubated with the cells for 5 minutes at 37℃. Calcein is a biological inert green-fluorescent molecule of a molecular mass of 623 Da and an estimated molecular radius of 0.6 nm [50]. TiO_2 NP solution containing the calcein dye was then removed and cells were rinsed twice with PBS to remove possible remnants of calcein dye in the extracellular solution. The cells were subsequently stained with a fluorescent nucleus dye, hoechst (10 μM) (Sigma-Aldrich, MO, USA), for 5 mintues at 37℃ and thoroughly rinsed again [14]. Fresh Hanks' solution was added into each well before taking fluorescent images of calcein and hoechst loaded cells with a Nikon fluorescence microscope. A percentage of calcein loaded cells against total number of

cells, as indicated by hoechst fluorescence, was calculated for each of the TiO_2 NP concentrations used in the experiment.

6. Mucin secretion and ELLA Preparation

The cells were seeded at 2×10^5 cells per well in a 24-well plate and cultured for 24 hrs. ChaGo-K1 cells were then rinsed with PBS and treated with BAPTA-AM (Invitrogen, CA, USA), thapsigargin (Sigma-Aldrich, MO, USA) or ryanodine (Sigma-Aldrich, MO, USA) for at least 30 minutes. Afterward the cells were stimulated for 15 minutes with the corresponding TiO_2 NP concentrations (0.75 mg/ml, 0.5 mg/ml, 0.25 mg/ml, and 0.1 mg/ml) or ionomycin (1 μM) (positive control) (Sigma-Aldrich, MO, USA), both prepared in PBS. The supernatant containing secreted mucin was collected and briefly centrifuged at 8,000 rpm to remove the residual TiO_2 NPs. The supernatant was then incubated in a 96 well (Nunc MaxiSorp, VWR, CA, USA) plate overnight at 4℃. Afterward the 96-well plate was washed with PBST (PBS + 0.05% Tween-20) and then blocked with 1% BSA. The 96 well plate was washed again with PBST and incubated with lectin (Wheat germ agglutinin, WGA) (Sigma-Aldrich, MO, USA), conjugated to horseradish peroxidase (HRP; 5 μg/ml) (Sigma-Aldrich, MO, USA), at 37℃ for 1 hr. The substrate, 3,3′,5,5′-Tetramethylbenzidine (TMB; Sigma-Aldrich, MO, USA), was added to each well at room temperature followed by H_2SO_4 (Sigma-Aldrich, MO, USA) in order to terminate the reaction. The optical density was measured at 450 nm [51].

7. Image Analysis

After staining the treated cells, image analysis was performed with an inverted Nikon Eclipse TE2000-U fluorescent microscope. Each photo was taken at a magnification of 200× and analyzed using SimplePCI (Compix Inc., Imaging Systems, Sewickle, PA, USA). The data shown is a representative of Ca^{2+} signals of more than 200 cells.

8. Statistical Analysis

The data was presented as means$\pm$SD. Each experiment was performed independently at least three times. Statistical significance was determined using a Student's t-test analysis with p values < 0.05 (GraphPad Prism 4.0, GraphPad Inc, CA, USA).

RESULTS

TiO_2 NP characterization

Dynamic laser scattering (DLS) was used to characterize the TiO_2 NPs. The particle size distribution ranged from ~9 to 80 nm due to minor aggregation or agglomeration while the predominant size is ~50 nm (Fig. 1A).

TiO_2 NPs induce cytosolic Ca^{2+} concentration increase

To investigate whether TiO_2 NPs could generate an increase in $[Ca^{2+}]_C$, ChaGo-K1 cells were loaded with Rhod-2 AM dye and exposed to 0.05 - 1 mg/ml of TiO_2 NPs. The change in $[Ca^{2+}]_C$, as represented by the fluorescence intensity within ChaGo-K1 cells, was monitored for 60 seconds. Figure 1B shows that 1 mg/ml of TiO_2 NPs induced an approximate 150 % increase, while lower TiO_2 concentrations (< 0.1 mg/ml) caused a minor elevation (~ 110 %) in $[Ca^{2+}]_C$ when compared with untreated cells. The effect of TiO_2 treatment on the $[Ca^{2+}]_C$ of ChaGo-K1 cells followed a concentration-dependent manner (Fig. 1B).

Extracellular source for Ca^{2+} increase

To determine the main source of elevated $[Ca^{2+}]_C$ upon stimulation, ChaGo-K1 cells were exposed to TiO_2 NPs in Ca^{2+}-free Hanks' solution. EGTA (2 mM) was added in Hanks' solution to chelate possible traces of Ca^{2+}. TiO_2 (0.05 mg/ml - 1 mg/ml) treatment under Ca^{2+}-free conditions failed to instigate a significant increase in $[Ca^{2+}]_C$ (Fig. 2A). Our data suggests that the extracellular Ca^{2+} pool is the primary source of the observed cytosolic Ca^{2+} increase. We then tested whether TiO_2 NPs can induce a Ca^{2+} influx via membrane channels. Blocking the channels with $CdCl_2$ (200 μM) significantly inhibited an increase in $[Ca^{2+}]_C$ (Fig. 2B). Co-treatment of cells with TiO_2 NPs and nifedipine greatly blocked the NP-induced $[Ca^{2+}]_C$ increase (Fig. 2C). However, the incomplete blockage of extracellular Ca^{2+} influx via channels postulates additional Ca^{2+} leakage through perturbed cell membranes. To confirm whether TiO_2 can instigate membrane disruption, thereby permitting unspecific extracellular Ca^{2+} entry, cytosolic leakage was assessed using the fluorescent calcein dye. It was found that the dye permeation ratio

increased from approximately 4 to 13 % with elevated TiO_2 concentrations ranging from 0.1 to 1 mg/ml (Fig. 2D).

Oxidative stress induced Ca^{2+} influx

To demonstrate that TiO_2-evoked $[Ca^{2+}]_C$ increase can be associated with oxidative stress, cells were pretreated with an anti-oxidant, N-acetylcysteine (NAC) [43]. Pre-treatment with NAC was able to partially attenuate the increase in cytosolic Ca^{2+} level triggered by 1 mg/ml and 0.75 mg/ml TiO_2 exposure (Fig. 2E). These results support the idea that oxidative stress, induced by TiO_2 NPs, contributes to the observed $[Ca^{2+}]_C$ increase and promote Ca^{2+}-dependent mucin secretion.

The ER as an intracellular source of Ca^{2+}

In order to determine the involvement of ER Ca^{2+} pool, it was depleted by pre-incubating the cells with thapsigargin. Pre-treatment with thapsigargin impeded TiO_2 NPs from triggering a sustained increase in the cytosolic Ca^{2+} level (Fig. 3A). We then investigated the role of the CICR mechanism by blocking RYRs (ryanodine receptors) [36]. Our results revealed that CICR was largely inhibited by ryanodine (a blocker for RYR associated with the CICR response) resulting in a significantly diminished $[Ca^{2+}]_C$ increase induced by NPs (Fig. 3B).

Ca^{2+}-dependency of TiO_2-induced mucin secretion

Enzyme-linked lectin assay (ELLA) was used to assess the amount of mucin secreted from ChaGo-K1 cells when stimulated with TiO_2 NPs. When compared to the control, TiO_2 NPs increased mucin secretion by 113%, 125%, 133%, 137% and 150% at 0.05, 0.1, 0.25, 0.5 and 0.75 mg/ml, respectively (Fig. 4A). Chelating the intracellular Ca^{2+} with BAPTA-AM yielded a significant reduction in mucin secretion (Fig 4B). Addition of thapsigargin (Fig. 4C) or ryanodine (Fig. 4D) also resulted in diminished mucin secretion induced by TiO_2 NPs. Our data indicates that TiO_2-induced mucin secretion is dependent on the $[Ca^{2+}]_C$, attributed to both external and internal Ca^{2+} pools (Fig. 4A-D). Ionomycin (a Ca^{2+} ionophore) was used to elicit mucin secretion as a positive control (Fig. 5).

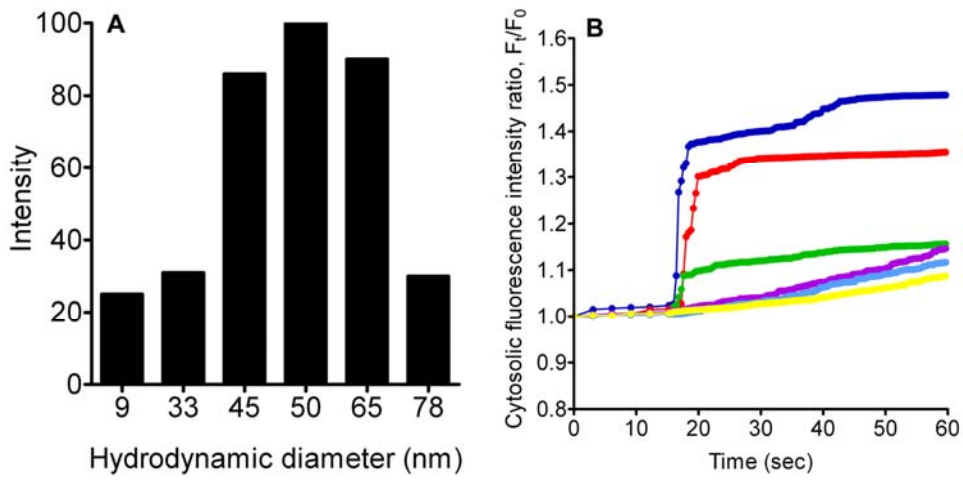

Figure 1. TiO_2 NP characterization and resultant $[Ca^{2+}]_C$ changes after NP treatment. A) DLS assessment of TiO_2 NPs in Hanks' solution showed a size distribution of ~9 to 80 nm. B) Cells were treated with TiO_2 NPs with concentrations of 0.05 mg/ml (yellow), 0.1 mg/ml (Light Blue), 0.25 mg/ml (Purple), 0.5 mg/ml (Green), 0.75 mg/ml (Red), and 1mg/ml (Blue) in normal Hanks' solution. Each line represents the average fluorescence intensity of approximately 200 cells per well.

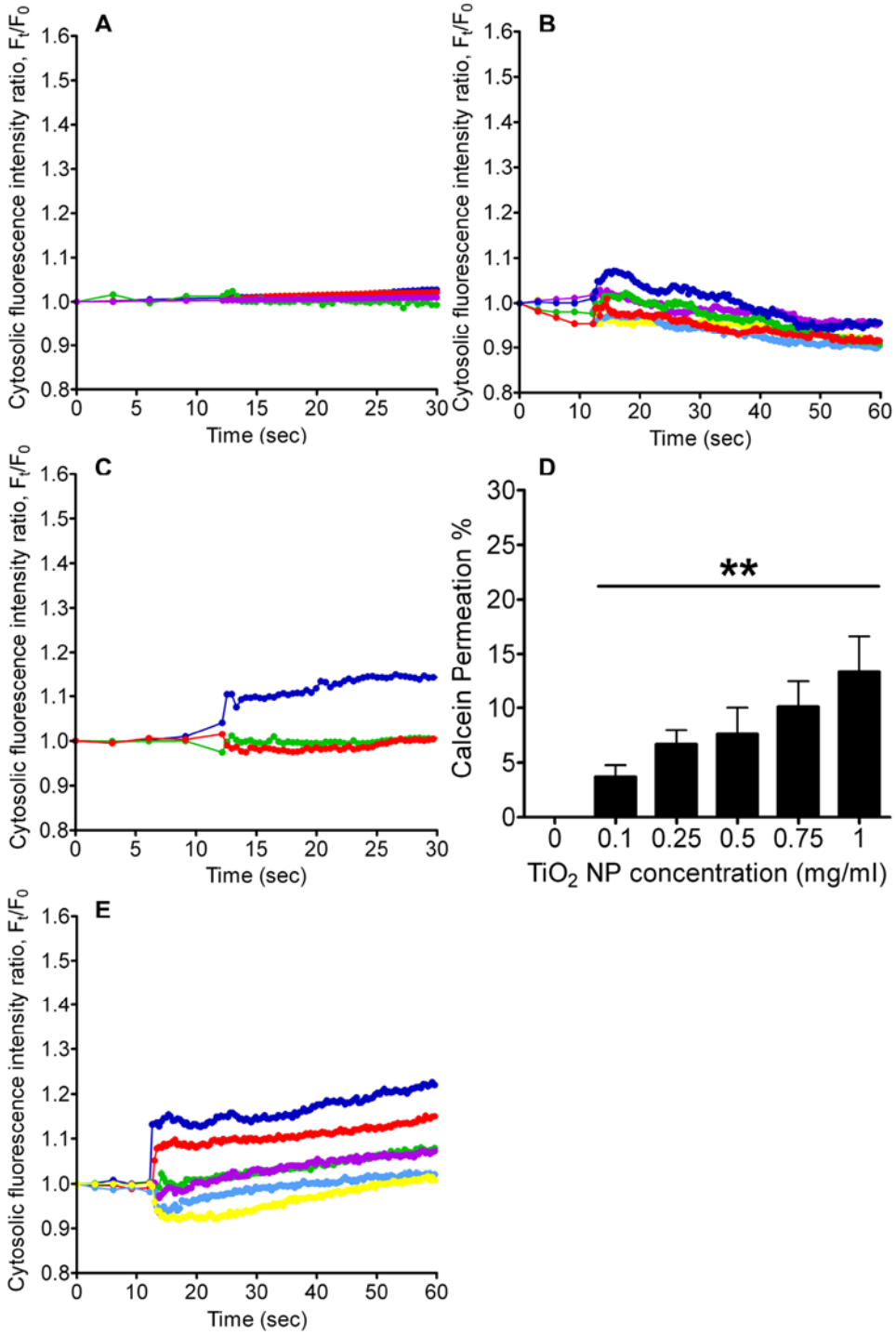

Figure 2. Measurement of the $[Ca^{2+}]_C$ and calcein dye leakage after TiO_2 NP treatment. Cells were treated with TiO_2 NPs with concentrations ranging from 0.05 mg/ml – 1 mg/ml, in A) Ca^{2+}-free Hanks' solution, B) in the presence of $CdCl_2$ (200 μM), C) nifedipine (10 μM), D) calcein (50 μM) (n = 12, **P < 0.005), and E) NAC (250 μM) (colors are as depicted in Figure 1B).

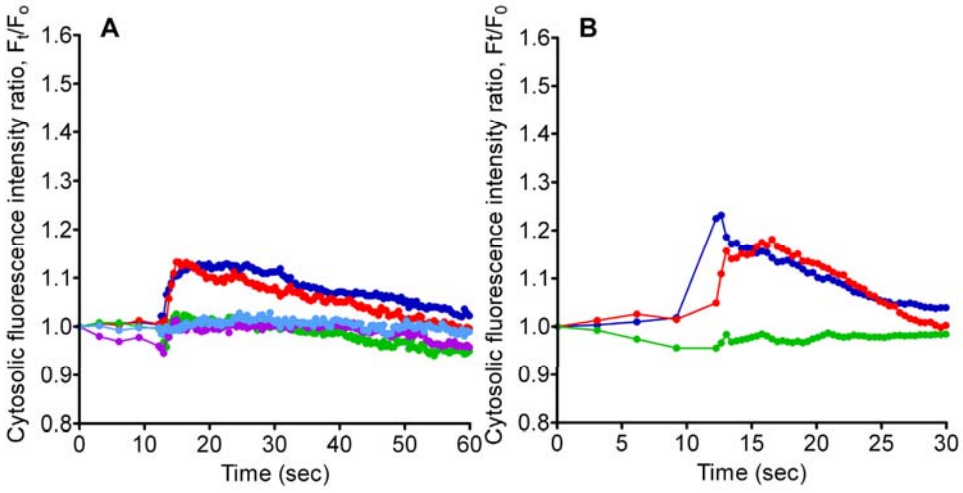

Figure 3. Measurement of $[Ca^{2+}]_C$ after stimulation by TiO_2 NPs. Cells were treated with TiO_2 NPs with concentrations ranging from 0.1 mg/ml – 1 mg/ml, in the presence of A) thapsigargin (100 nM), and B) ryanodine (100 μM) (colors used are consistent with Figure 1).

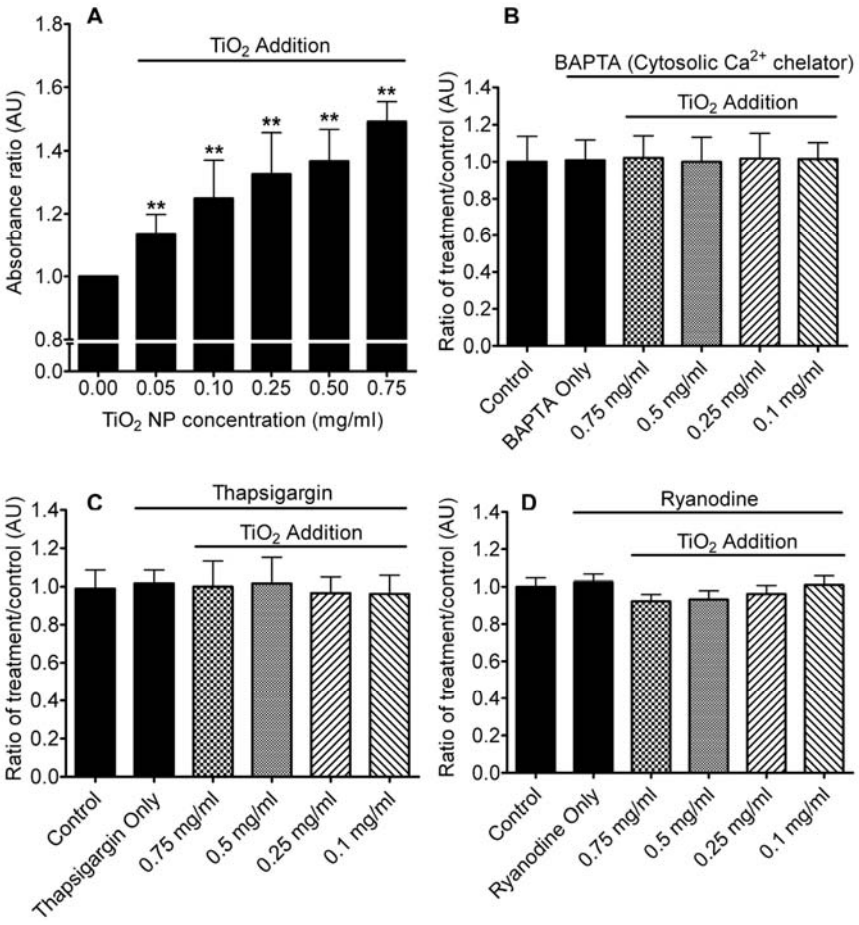

Figure 4. Measurement of mucin secretion triggered by TiO_2 NPs. Cells were treated with TiO_2 NP concentrations ranging from 0.05 mg/ml - 0.75 mg/ml. Figure 4A) shows the relative quantification of mucin secreted after TiO_2 stimulation under normal conditions ($n \geq 7$, $^{**}P < 0.005$), 4B) in the presence of BAPTA-AM (50 μM) ($n \geq 9$), 4C) with pre-treatment of thapsigargin (100 nM) ($n \geq 8$), 4D), and with ryanodine (100 μM) ($n \geq 5$).

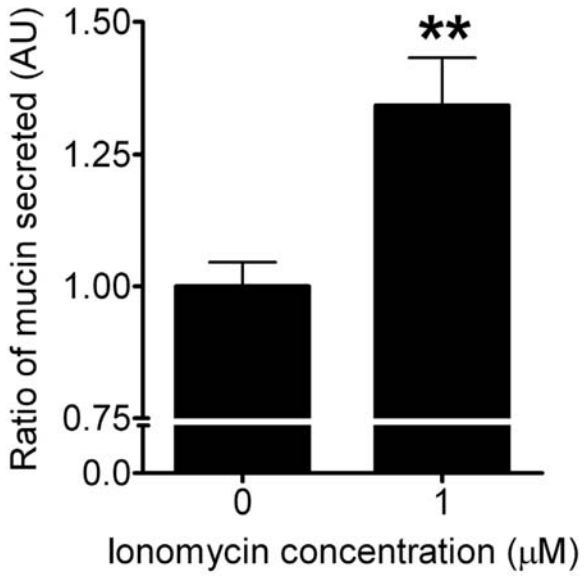

Figure 5. Mucin secretion in response to ionomycin application (positive control, $n \geq 3$). Concentration of ionomycin used was 1 μM.

DISCUSSION

Recently, an increasing number of reports have shown that airborne particulate pollution found in both the ambient and working environments, particularly TiO_2 NPs, can exacerbate airway diseases [20,21,22,23,24,25,29,30,52]. Aggravated clinical manifestations of COPD, CF and asthma may include intensified symptoms of mucociliary transport impairment and mucus hypersecretion [16,34]. The resultant accumulation of thick obstructive mucus usually occupies airway lumen, thereby limiting airflow and leading to morbidity [16,34]. Despite documentations of TiO_2-induced cellular nanotoxicity effects, pulmonary inflammatory responses and emphysema-like pathology [31], whether TiO_2 NPs can directly trigger mucin secretion has not been resolved. In this study, we demonstrate that TiO_2 NPs can stimulate mucin secretion from bronchial epithelial ChaGo-K1 cells via a Ca^{2+}- dependent pathway.

Our study showed that TiO_2 NPs can induce mucin secretion that increases as a function of TiO_2 NP concentration (Fig. 4A). The TiO_2 concentration range used in our study is consistent with previous reports representing the concentration found in ambience and nanotechnology industries [46,53,54,55]. While NP exposure has been long associated with increasing mucin synthesis due to goblet cell hyperplasia [32], our study indicates that TiO_2 NPs can directly trigger mucin secretion in the airway.

It has been well established that intracellular Ca^{2+} plays a vital role in stimulus-secretion coupling [56]. Previous reports have documented that an elevated $[Ca^{2+}]_C$ precedes mucin granule exocytosis [18]. NP exposure has been shown to trigger an intracellular Ca^{2+} increase in various cells; therefore, we examined the cellular Ca^{2+} signaling pathway involved during TiO_2 stimulation [41,44,57]. At TiO_2 concentrations of 0.5, 0.75, and 1 mg/ml, there was a sustained elevation in $[Ca^{2+}]_C$. At lower doses (0.05, 0.1 and 0.25 mg/ml), the $[Ca^{2+}]_C$ increased gradually within the 1st minute (Fig. 1B). Our data demonstrated that TiO_2 NPs induced a concentration dependent increase in $[Ca^{2+}]_C$, which is consistent with results from the mucin secretion measurements (Fig. 4A).

The stimulus-induced intracellular Ca^{2+} signal can be evoked by the entry of Ca^{2+} through voltage-gated Ca^{2+} channels, or by the release of Ca^{2+} from intracellular Ca^{2+} stores [56,58,59]. Previous researches have suggested that extracellular Ca^{2+} influx plays an important role in the elevated $[Ca^{2+}]_C$ during NP stimulation [41,43,44,60]. Data from experiments performed in Ca^{2+}-free Hanks' solution confirmed that $[Ca^{2+}]_C$ failed to increase when treated with TiO_2 NPs (Fig. 2A). To characterize the nature of the Ca^{2+} influx induced by TiO_2 NPs, we first evaluated the effect of cadmium chloride ($CdCl_2$), a general Ca^{2+} channel blocker [48,61]. Figure 2B shows that the $[Ca^{2+}]_C$ remained low and relatively unchanged with $CdCl_2$. Secondly, nifedipine, a widely used L-type Ca^{2+} channel blocker, markedly diminished the increase in $[Ca^{2+}]_C$ (Fig. 2C). The effect of nifedipine implies that TiO_2 NPs can activate L-type voltage gated Ca^{2+} channels, allowing extracellular Ca^{2+} influx into the cytosol. This observation is consistent with previous reports showing that ultrafine carbon black and ZnO NP-induced $[Ca^{2+}]_C$ elevation can also be attenuated by nifedipine [43,44]. In addition, several reports have suggested that oxidative stress induced by NPs can exert an impact on the intracellular Ca^{2+} signaling pathway and that the activity of Ca^{2+} channels may be altered by ROS [43,44,57]. Results from Figure 2E showed that NAC significantly reduced the rising $[Ca^{2+}]_C$ generated by TiO2 NPs. Huang et al, has also demonstrated that NAC can attenuate the intracellular Ca^{2+} level when challenged with ZnO NPs [43]. Our results support the idea that NAC and other antioxidants may be effective in reducing NP-instigated mucin hypersecretion. NPs such as TiO_2 can damage cell membrane integrity by possible lipid peroxidation [43,47], thereby creating pores on the lipid bilayer [62] that may allow the transient influx of extracellular Ca^{2+}. Our data further demonstrated that co-adminstration of TiO_2 NPs and fluorescent calcein dye lead to intracellular leakage and the permeation efficiency increased in a TiO_2 concentration dependent manner (Fig. 2D). Calcein has also been previously utilized to evaluate the efficacy of peptides in causing membrane perturbation [63]. Our result suggests that the possible membrane perturbation/transient pore formation induced by TiO_2 NPs allows an extracellular Ca^{2+} influx and may account for the portion of Ca^{2+} that can not be completely abolished by blocking L-type Ca^{2+} channels with nifedipine.

Increasing the $[Ca^{2+}]_C$ of human goblet cells has been shown to trigger degranulation [18]. We used BAPTA (cytosolic Ca^{2+} chelator) to test whether the increase in Ca^{2+} induced by TiO_2 NPs could stimulate mucin exocytosis. It is evident that BAPTA significantly inhibited mucin exocytosis (Fig. 4B), indicating that TiO_2 NPs can elicit a $[Ca^{2+}]_C$ increase, thereby leading to mucin secretion.

Besides the external Ca^{2+} source (Hanks' solution), the ER is one of the major internal Ca^{2+} stores. Figures 3A and 4C revealed that when the ER Ca^{2+} had been depleted by pretreatment with thapsigargin, the TiO_2 NP-induced $[Ca^{2+}]_C$ failed to increase significantly, and the subsequent mucin secretion was abolished. Our data indicates that the ER plays a critical role in relaying TiO_2-induced Ca^{2+} signaling. CICR is a positive feedback mechanism where the ER amplifies a small increase in $[Ca^{2+}]_C$, (e.g. due to voltage-gated Ca^{2+} influx [38]), with the activation of RYRs that will lead to the release of more Ca^{2+} from the ER [35,36]. Previous studies have shown that through activation of RYRs with Ca^{2+}, CICR can generate an overall increase in $[Ca^{2+}]_C$ [36,37,38]. Our data showed that ryanodine inhibited a continual rise in $[Ca^{2+}]_C$ when applying TiO_2 NPs (Fig. 3B). Therefore, it is indicative that the TiO_2-instigated increase in $[Ca^{2+}]_C$ was also CICR dependent. The effect of ryanodine was further demonstrated by the lack of mucin secretion under TiO_2 NP stimulation (Fig. 4D).

In summary, our study indicates that cellular exposure to TiO_2 NPs can activate membrane L-type Ca^{2+} channels, induce ROS production and possibly disrupt the cellular membrane. Influx of extracellular Ca^{2+} into the cytoplasm raises $[Ca^{2+}]_C$, which in turn can trigger ryanodine receptors on the ER to release ER resident Ca^{2+} via the CICR mechanism. A sufficient increase in the cytosolic Ca^{2+} level results in subsequent mucin secretion. More importantly, our results provide a direct link between airborne particulate matters and the pathogenesis of chronic airway diseases involving mucus hypersecretion and airway obstruction. In addition, we demonstrate that once thought inert and harmless TiO_2 NPs can indeed interfere with intracellular Ca^{2+} signaling, possibly leading to pathological states.

CHAPTER 3

Functionalized Positive Nanoparticles Reduce Mucin Swelling and Dispersion

ABSTRACT

Multi-functionalized nanoparticles (NPs) have been extensively investigated for their potential in household and commercial products, and biomedical applications. Previous reports have confirmed the cellular nanotoxicity and adverse inflammatory effects on pulmonary systems induced by NPs. However, possible health hazards resulting from mucus rheological disturbances induced by NPs are underexplored. Accumulation of viscous, poorly dispersed, and less transportable mucus leading to improper mucus rheology and dysfunctional mucociliary clearance are typically found to associate with many respiratory diseases such as asthma, cystic fibrosis (CF), and COPD (Chronic Obstructive Pulmonary Disease). Whether functionalized NPs can alter mucus rheology and its operational mechanisms have not been resolved. Herein, we report that positively-charged functionalized NPs can hinder mucin gel hydration and effectively induce mucin aggregation. The positively-charged NPs can significantly reduce the rate of mucin matrix swelling by a maximum of 7.5 folds. These NPs significantly increase the size of aggregated mucin by approximately 30 times within 24 hrs. EGTA chelation of indigenous mucin crosslinkers (Ca^{2+} ions) was unable to effectively disperse NP-induced aggregated mucins. Our results have demonstrated that positively-charged functionalized NPs can impede mucin gel swelling by crosslinking the matrix. This report also highlights the unexpected health risk of NP-induced change in mucus rheological properties resulting in possible mucociliary transport impairment on epithelial mucosa and related health problems. In addition, our data can serve as a prospective guideline for designing nanocarriers for airway drug delivery applications.

Keywords: Nanoparticles; mucin aggregation; nanoparticle-mucin complex; swelling kinetics

INTRODUCTION

A myriad of functionalized-NPs have been used to develop commercial commodities in various industrial sectors. They are heavily implemented in the manufacturing of paint, carpet, paper, plastic, textiles, clothes and cosmetics [46,64,65,66]. NPs also play major roles in decontaminating aqueous wastes and food processing [66,67,68]. Recent developments in the pharmaceutical field focus on nanocarriers that transport drugs or genes to targeted areas via inhalation to treat numerous respiratory and systemic diseases [27,69]. The pulmonary route proves to be an important site of nano-drug (e.g. aerosolized nanopowder) and therapeutic gene delivery that offers both local and systemic targeting for treatment of many diseases [27,70]. Even in major respiratory diseases, such as pulmonary tuberculosis, cystic fibrosis (CF), Chronic Obstructive Pulmonary Disease (COPD) and bronchial asthma, nanocarriers have shown promising therapeutic effects *in vitro* and in animal experiments [70,71].

Due to their diverse applications, recurrent aerosolized exposure to these NPs are anticipated, yet the potential health risks brought about by NPs are not fully understood [72]. Epidemiological studies have confirmed a positive correlation between levels of particulate pollution and increased morbidity and mortality rates among general populations [21,52]. The adverse health effects seem to be dominated by pulmonary symptoms. For instance, many reports have addressed that occupational exposure of inhaled NPs can lead to respiratory diseases such as pneumoconiosis (pulmonary fibrosis) and bronchitis [73,74]. Increasing inhalation of ambient ultrafine particles has been linked with exacerbation of respiratory symptoms and mortality among COPD sufferers [22,75,76]. It has also been documented that NPs can instigate oxidative stress and cellular toxicity in various types of cells [27,43]. For instance, in human bronchial epithelial cells, we have previously demonstrated that titanium dioxide NP exposure resulted in cell death without photoactivation [46]. In addition, polystyrene NPs have been shown to induce lung inflammation [77].

Mucus rheology plays a critical role in maintaining respiratory health. Mucins are large, highly glycosylated proteins [1,2]. The polyanionic nature of mucin stems primarily from

sialic acid, sulfate, and carboxyl (COO^-) groups present in these linked oligosaccharides. Beside physical entanglement, cationic calcium ions can act as crosslinkers that condense the mucin matrices inside mucin granules before exocytosis [2]. Upon release, phase transition mainly driven by the Donnan effect triggers the massive decondensation of mucin networks [2]. Hydrogen bonding, hydrophilic and hydrophobic interactions have also been proposed to contribute to the gel properties of mucin [2]. The gel characteristics and rheological properties of mucin are critical for maintaining the integrity of epithelia by trapping bacteria and viruses for mucociliary clearance.

The clinical manifestation of major respiratory diseases (i.e. COPD [17], asthma [15] and CF [78]) are related to thick mucus. The relationship between mucin dehydration and defective mucus clearance has been well established [79,80,81]. As a result, the poorly hydrated, highly viscous and less transportable mucus appears to accumulate within airway passages [15,16]. Obstruction of airway lumen with viscous mucus is usually accompanied by chronic bacterial infection, inflammation and impaired mucociliary transport [16,17]. Chronic exposure to NPs can potentially predispose humans to lung inflammation and increase the risk of COPD [20,76]. However, whether NPs can alter the viscoelastic property of mucus and lead to concomitant pathological outcomes is not clear. Despite evidence on NP-induced cellular nanotoxicity, studies addressing the link between the surface property of NPs and their harmful effects are still lacking. Our research examined the relationship between NP surface modifications and alteration in mucus rheological properties. The concentration range of NPs used in this investigation was within the level found in ambience and in nanotechnology industries [77,82]. In this study, we found that positively-charged NPs can promote mucin aggregation, thereby reducing the rate of mucin gel expansion via crosslinking polyanionic mucin matrices. Our results provide the first mechanistic link between NP exposure and viscous mucus accumulation commonly found in pulmonary diseases.

MATERIALS AND METHODS

1. A549 cell culture

The human lung carcinoma cell line A549 was obtained from American Type Culture Collection (ATCC, VA, USA). A549 cell line is an airway epithelial cell line commonly used as a secretory model [83]. Cells were cultured in 15 cm cell culture plates (VWR, CA, USA) containing F-12 nutrient mixture medium (Invitrogen, CA, USA) that was supplemented with 100 U of penicillin/streptomycin and 10% heat-inactivated fetal bovine serum (FBS) (Invitrogen, CA, USA). The A549 lung cells were cultured in 15 cm Falcon plates and incubated in a humidified incubator at 37℃/5% CO_2. Cell counts were performed using trypan blue (Sigma-Aldrich, MO, USA) exclusion and a Bright-Line haemocytometer.

2. Nanoparticle preparation

Carboxyl-, amine- and non-functionalized polystyrene particles with various sizes (i.e. 57 nm, 99 nm, 120 nm and 160 nm) (Bangs Laboratories, Fishers, IN, USA) were used in our study. All NPs have a size standard deviation of $\leq$ 10% (based on manufacturer information). These sizes were independently confirmed using homodyne dynamics laser scattering. All nanoparticle samples were sonicated before usage.

3. Particle sizing using dynamic laser scattering

The aggregation of mucus was monitored by measuring particle size using homodyne dynamics laser scattering (DLS). Samples of porcine gastric mucin at 1 mg/L (Sigma-Aldrich, MO, USA) were prepared with Hanks' solution containing 1.2 mM Ca^{2+}, 20 mM Tris-HCl (tris(hydroxymethyl)aminomethane hydrochloride) and 10 mM MES (2-(N-morpholino)ethanesulfonic acid) (Sigma-Aldrich, MO, USA) to buffer the pH around 7.4 [14]. The solution was thoroughly mixed until mucin has dissolved. Aliquots of mucin samples (10 ml) were directly filtered through a 0.22-μm Millipore PES membrane (pre-washed with 0.1N HCl) (Fisher Scientific, CA, USA) into clean scintillating vials. The scintillating vials were positioned in the goniometer of a Brookhaven laser spectrometer (Brookhaven Instruments, NY, USA). Mucin gel aggregation was allowed to take place by equilibrating with three filtered types of NPs each expressing different surface

modifications for 72 hrs; they were subsequently analyzed by detecting the scattering fluctuations at a 45 degree scattering angle. Commercialized polystyrene NPs (Bangs Laboratories, Fishers, IN) with dimensions of 57, 99, 120 and 160 nm were added to mucin samples. Positive (-NH_2 based, 57 and 160 nm), negative (-COOH, 120 nm) and non-functionalized (hydrophobic, 99 nm) surface charges were used in this study. All NPs were prepared in suspension of Hanks' solution (buffered with Tris-HCl/MES at pH 7.4). Filtered NP solution, added to scintillating vials, was tested for its ability to promote mucin aggregation and was monitored at 1 hr, 3 hrs, 5 hrs, 24 hrs, 48 hrs and 72 hrs. Self aggregation induced by NP-only and mucin-only controls were monitored at 1 hr, 24 hrs, 48 hrs and 72 hrs. The pH was also monitored and maintained at approximately 7.4 during the experiments. The autocorrelation function of the scattering intensity fluctuations was averaged over a 3-min sampling time using a Brookhaven BI 9000AT autocorrelator. Particle size distribution was calculated by CONTIN [84]. Calibration was conducted with standard monodisperse suspensions of latex microspheres ranging from 50 nm to 10 μm (Polysciences, PA, USA).

4. Scanning electron microscopy (SEM)

Samples of porcine gastric mucin at 1 mg/L (Sigma-Aldrich, MO, USA) were prepared with Hanks' solution (buffered with Tris-HCl/MES at pH 7.4) and incubated with 10 mg/L of positively-charged 57 and 160 nm NPs. After incubation for 5 hrs or 72 hrs, 5 ml of mucin were filtered through a 0.22-μm Millipore isopore membrane (Fisher Scientific, CA, USA). The filtered mucin was subsequently fixed with 4% paraformaldehyde (prepared in PBS at pH 7.4) (Sigma-Aldrich, MO, USA) for 5 min, followed by careful rinsing with Hanks' solution twice. The fixed mucin and NP complexes were dehydrated by soaking in serially diluted ethanol (35%, 50%, 70%, 95% and 100% ethanol) for 5 min. The specimens were air dried and examined with FEI Quanta 200 ESEM (North America NanoPort, OR, USA).

5. EGTA dispersion of aggregated mucin

EGTA (Ethylene glycol-bis(2-aminoethylether)-N,N,N′,N′-tetraacetic acid, 2 mM) (Sigma-Aldrich, MO, USA) was used to disperse aggregated mucus, which was

monitored by measuring particle size by homodyne dynamics laser scattering. Samples of porcine gastric mucin at 1 mg/L (Sigma-Aldrich, MO, USA) were prepared with Hanks' solution containing 1.2 mM Ca^{2+} (buffered with Tris-HCl/MES at pH 7.4) and thoroughly mixed until mucin has dissolved. Aliquots of mucin samples (10 ml) were directly filtered through a 0.22-μm Millipore PES membrane (pre-washed with 0.1N HCl) (Fisher Scientific, CA, USA) into clean scintillating vials. The scintillating vials were positioned in the goniometer of a Brookhaven laser spectrometer (Brookhaven Instruments, NY, USA). Mucin gel aggregation was initiated by incubating mucin samples with filtered positively-charged NPs (-NH_2 based 57 and 160 nm) (Bangs Laboratory Inc, Fishers, IN) and were monitored after 1, 3, 5, 24, 48 and 72 hrs. EGTA (2 mM) was subsequently applied to already aggregated mucin solution after 72 hrs. The change in aggregation size was detected for another 72 hrs. The pH was also monitored and maintained at approximately 7.4 during the experiments. The autocorrelation function of the scattering intensity fluctuations was averaged over a 3-min sampling time, using a Brookhaven BI 9000AT autocorrelator. Particle size distribution was calculated by the CONTIN [84]. Calibration was conducted with standard monodisperse suspensions of latex microspheres ranging from 50 nm to 10 μm (Polysciences Inc, PA, USA).

6. Swelling kinetics of exocytosed mucin matrices

The A549 cell culture plates were rinsed with Hanks' buffer twice. Non-trypsin dissociation buffer (Invitrogen, CA, USA) was added to detach cells from the plates and were subsequently incubated at 37° C for 15 minutes, centrifuged at 700 rpm for 5 min, and resuspended in Hanks' solution (Invitrogen, CA, USA) (buffered with Tris-HCl/MES at pH 7.4). Cells were resuspended into MatTek glass bottom dishes (MatTek Corporation, MA, USA) and equilibrated in a 37°C incubator for 10 minutes prior to adding 10 mg/L and 1 mg/L of 160 and 57 nm positively-charged NPs (Bangs Laboratories, Fishers, IN). The pH was monitored and maintained at approximately 7.4 throughout the experiments.

A549 cells were viewed and video-recorded with phase-contrast lens using a Nikon Eclipse TE-2000-U inverted fluorescence microscope (Nikon Eclipse TE-2000U, Tokyo,

Japan). Degranulation of A549 cells was induced by 1 uM ionomycin (Sigma-Aldrich, MO, USA) and was found to be a readily observable discrete quantal process. During exocytosis into extracellular Hanks' solution, released granule matrices undergo rapid swelling. Video-recordings of granular exocytosis and swelling were captured at 30 frames s^{-1}.

Measurements of radii, of the released mucin matrices, as a function of time were used to verify that the swelling of the secreted material followed the characteristic features of polymer gel swelling kinetics [85,86]. The swelling of a polymer gel follows a typical diffusive kinetics that is independent of the size, internal topology, or chemical composition of the gel [86]. For spherical gels as observed from the exocytosed mucin granule matrices of A549 cells, the radial dimension increased following a characteristic first order kinetics of the form $r(t) = r_f - (r_f - r_i)\, e^{-t/\tau}$ (equation 1), where r_i and r_f are the initial and final radius of the secretory granule matrix, respectively, and τ is the characteristic relaxation time of the swelling process [2]. The polymer network of gels diffused into the solvent (Hanks' solution), with a diffusivity (D) ($D = (r_f)^2/\tau$ [$cm^2\ s^{-1}$]) (equation 2). The diffusivity (D) of polyionic gels varied with the concentration of counterions in the swelling medium.

7. Statistical Analysis

The data was presented as means$\pm$SD. Each experiment was performed independently at least three times. Statistical significance was determined using a Student's t-test analysis with p values of <0.005 (Microsoft Excel and GraphPad Prism 4.0, GraphPad Software, Inc., San Diego, CA, USA).

RESULTS

Positively-charged nanoparticle induces mucin aggregation

To understand the possible mechanisms of how surface charge modifications on NPs affect mucin rheological properties, we examined the effect of different NP surface charges on mucin aggregation and gelation. NPs with non-functionalized, positive, or negative surface charges were added to mucin samples to monitor the mucin gel size change with dynamic laser scattering (DLS) after 0, 1, 3, 5, 24, 48 and 72 hrs. DLS is a well established technique used to measure the hydrodynamic diameter of mucin gel aggregates [87]. In Figure 1A, it is clearly demonstrated that a steady concentration-dependent increase in mucin aggregate size was induced by positively-charged amine (-NH_2) polystyrene NPs (160 nm) at 1 mg/L and 10 mg/L. Positively-charged NPs (1 mg/L) caused mucin to aggregate from the original 240 nm to 1000 nm within 24 hrs and plateaued throughout 72 hrs. In comparison to the NP-only control (no mucin) at 1 mg/L, only minor aggregation was found throughout the 72 hrs (Figure 1D). On the other hand, 10 mg/L of positively-charged NPs induced a quick rise in mucin aggregation starting from the 1st hour (~2000 nm) to the 5th hour (~2900 nm). At the 24th hour, the average mucin gel size increased rapidly to around 5500 nm, while it plateaued around 72 hrs at 6300 nm (Figure 1A). Comparing the 10 mg/L treatment group to the mucin-only control (Figure 1G), there is a 19 and 24 time increase in mucin aggregate size in the corresponding 24 and 72 hrs. However, at much lower concentrations, positively-charged NPs (100 μg/L) failed to induce significant mucin aggregation (Figure 1A). In addition, multiple concentrations of negatively-charged (-COOH based, 120 nm) and non-functionalized (99 nm) NPs yielded a basal size of about 200 nm (Figures 1B & C). The results show that negatively-charged and non-functionalized NPs are not able to associate effectively with mucins (Figures 1B & C). Therefore, our data showed that only positively-charged NPs can effectively promote mucin aggregation. A NP size-dependent effect on mucin aggregation was subsequently investigated. Figure 1E illustrated positively-charged 57 nm NPs generated more pronounced mucin aggregates than 160 nm under the same conditions. The control experiment (Figures 1D & F) indicated that 10 mg/L of 160 and 57 nm positive charged NPs generated only slight self-clumping. Furthermore, 57 nm NP-induced mucin aggregates were approximately 30 times larger

than the mucin-only control (Figures 1E & G). The mucin-only control remained at the hydrodynamic diameter of about 200 nm throughout 72 hrs (Figure 1G). These results suggested that NP-induced mucus aggregation occurred mainly as a result of the interactions between NPs and mucin instead of self-aggregation of NPs or mucins.

SEM images of nanoparticles-induced mucin gel complex

To provide a visual representation that further establishes the relationship between NP concentrations and the size of mucin gels, aggregated mucin size was determined by SEM images. Mucin samples containing 10 mg/L of 57 nm and 160 nm positively-charged NPs were prepared. The resulting mucin gels were collected at 5 hrs and 72 hrs. Mucin gels were filtered through 0.22 μm Isopore membranes, fixed and imaged with SEM. Sizes of mucin aggregates presented in Figures 2A-D confirm the size measurements from DLS. It is also evident that longer incubation resulted in larger NP-mucin aggregates for 57 nm NPs (Figures 2B & D) and 160 nm NPs (Figures 2A & C), which is consistent with DLS measurements (Figures 1A & E). In addition, SEM images demonstrated that these aggregated mucin gels were associated with NPs forming NP-mucin gel complexes.

Positively-charged nanoparticles serve as mucin gel crosslinkers

Calcium ions have been shown to act as a vital crosslinker in the formation, stability and condensation of mucin gels [2]. Our previous results have shown that gels crosslinked by Ca^{2+} can be dispersed by Ca^{2+} chelators (e.g. EDTA) [84]. To further understand the role that positively-charged NPs play in promoting mucin aggregation and gelation, we tested whether positively-charged NPs can serve as crosslinkers replacing Ca^{2+} ions. Positively-charged NPs (10 mg/L) of 160 nm and 57 nm were added to mucin solution (1 mg/L) and incubated for 72 hrs before applying 2 mM EGTA (Ca^{2+} chelator). The pH was kept in a range of pH 7.4 by Tris-HCl and MES. The changes of aggregated mucin size were subsequently monitored after 3, 24, 48, and 72 hrs. Figures 3A & B demonstrated that calcium chelation by EGTA was unable to significantly reduce aggregated mucin size caused by 160 nm or 50 nm NPs. This result further supports the role of positively-charged NPs as Ca^{2+} crosslinkers.

Positively-charged nanoparticles retards mucin hydration rate

Knowing that positively-charged NPs can disturb mucin rheological properties, we then tested whether positively-charged NPs could impair mucin hydration by utilizing an *in vitro* mucin swelling kinetics functional assay (see methods). A representative graph comparing the swelling kinetics of newly exocytosed mucin networks, between the control and positively-charged NP treatment, is shown in Figure 4A. The evidence indicated that positively-charged NPs impeded the swelling rate (~hydration) of mucin networks (Figure 4A). Converting swelling rate into diffusivity (D) using equation (2) yielded similar results. The measurements showed that positively-charged NPs (10 mg/L) of 160 and 57 nm retarded the rates of mucin diffusivity approximately 3.6 and 7.5 times, while 1 mg/L of 160 and 57 nm decreased mucin diffusivity about 1.7 and 6.1 times, correspondingly, when compared to the control (NP free) (Figure 4B). Within the same category of NP size, there is also a concentration-dependent effect on reducing the rate of mucin diffusivity. Higher NP concentration (10 mg/L) yields a slower rate of mucin diffusivity than lower NP concentration (1 mg/L). Our data indicates that positively-charged NPs can reduce the rates of mucin hydration and diffusivity, possibly leading to an elevated mucus viscosity and dysfunctional mucociliary transport.

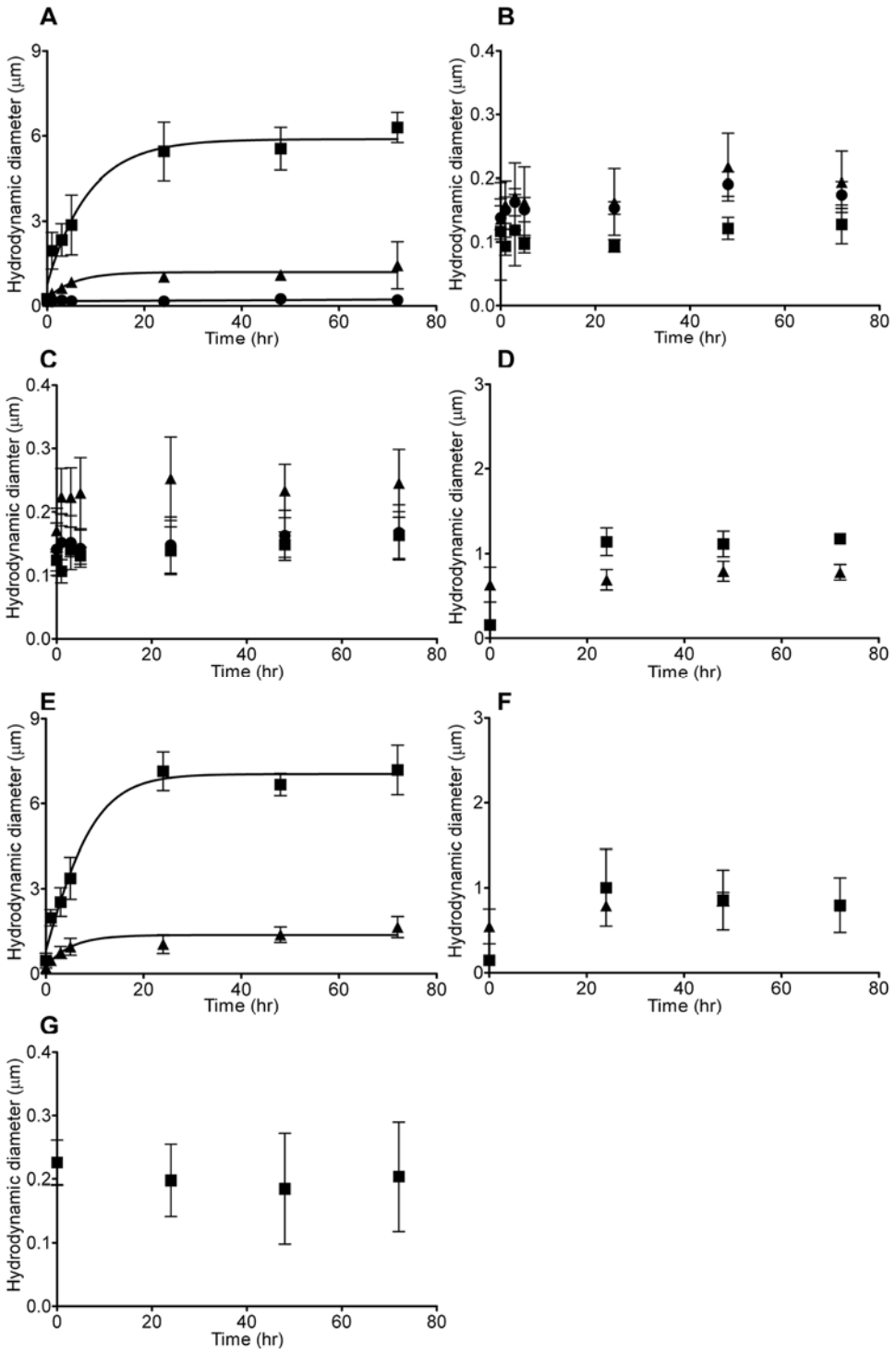
A
B
C
D
E
F
G
Hydrodynamic diameter (μm)
Time (hr)
0
20
40
60
80
0.0
0.1
0.2
0.3
0.4
1
2
3
6
9

Figure 1. Interaction of NPs and mucin aggregation. (A) Positively-charged NPs (160 nm) ($n \geq 6$) induce significant mucin aggregation while (B) negatively-charged (120 nm) ($n \geq 6$) and (C) non-functionalized NPs (99 nm) ($n \geq 6$) fail to induce mucin aggregation since the aggregate size remained below 300 nm throughout 72 hrs incubation. (D) Positively-charged NPs (160 nm) ($n \geq 5$) alone can not generate large aggregates in the same Hanks' solution. Smaller size positively-charged (57 nm) ($n \geq 6$) promote larger mucin aggregates (E). At the same time, negative controls show that (F) positively-charged NPs (57 nm) ($n \geq 5$) or (G) mucin alone (1 mg/L, $n \geq 5$) can not generate large aggregates. Various concentrations (solid circles: 100 μg/L, solid triangles: 1 mg/L, solid squares: 10 mg/L) of positively-charged, negatively-charged and non-functionalized NPs (160, 57, 120 and 99 nm) were added to mucin solution (1 mg/L). Significant mucin aggregates were found at 10 mg/L and 1 mg/L of positive NPs. The size of mucin-NPs aggregates were determined with DLS as described previously [87].

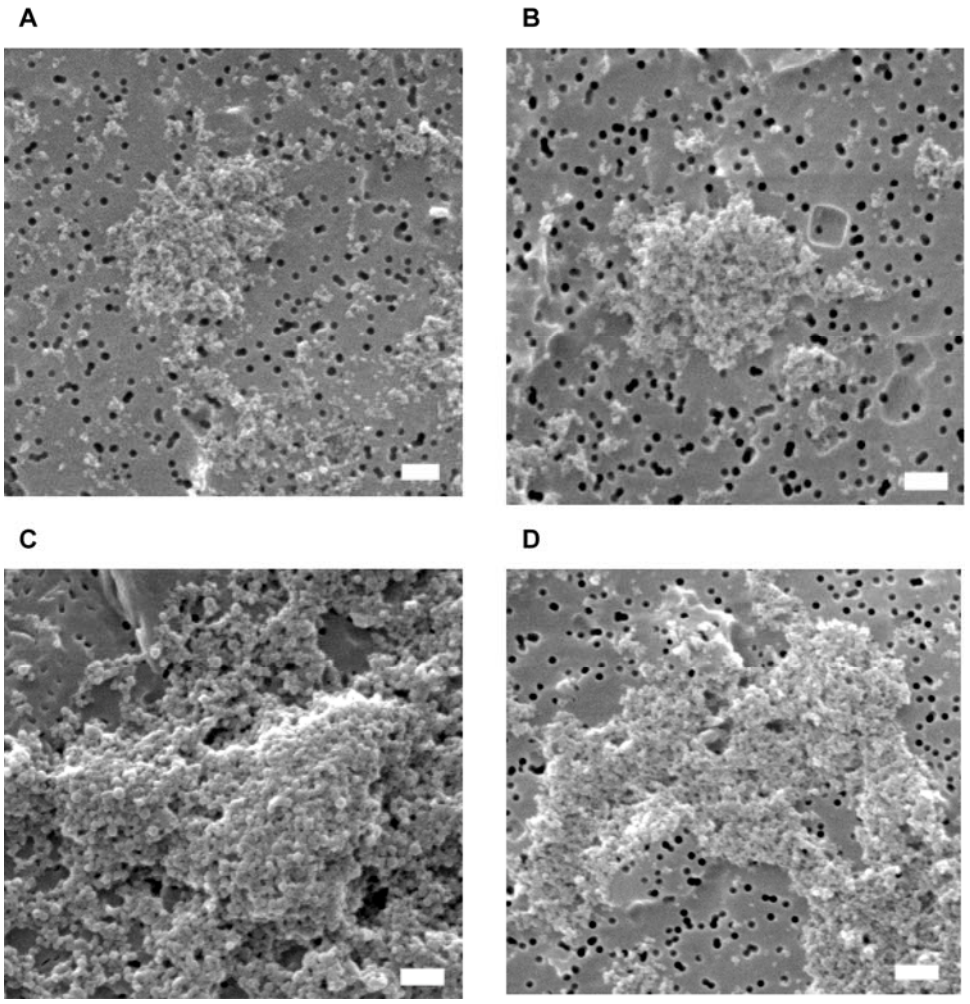

Figure 2. SEM images of mucin-NP complexes. SEM micrographs of mucin-NPs complexes with 160 nm (A, C) and 57 nm (B, D) positively-charged NPs after 5 hrs (A, B) and 72 hrs (C, D). These SEM images clearly demonstrate that NPs and mucins aggregate together forming large mucin-NPs gels. The black holes in the images are the pores in Isopore membranes. The scale bar is 1 μm.

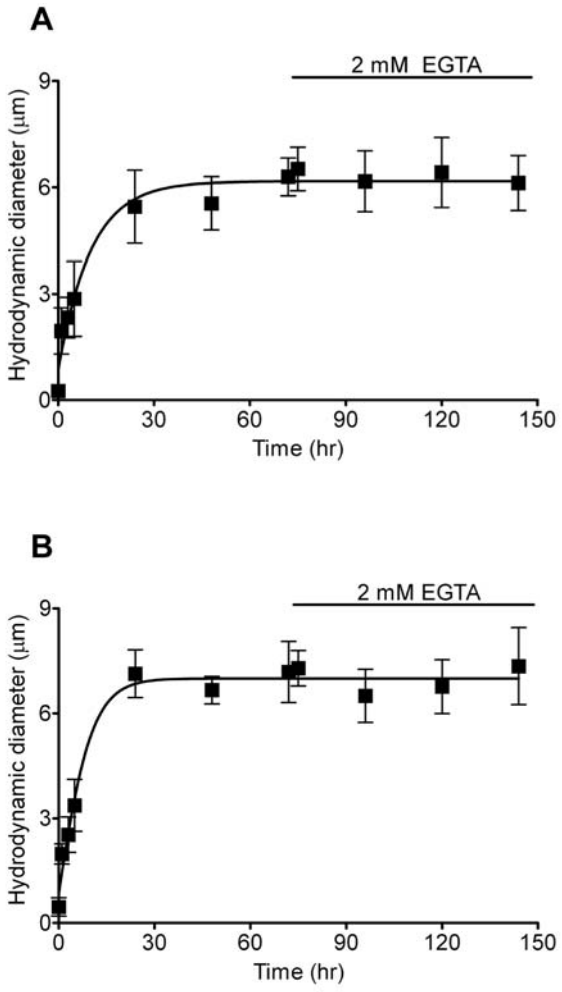

Figure 3. Inability of EGTA (Ca^{2+} chelator) to disperse NPs-induced mucin aggregates. Positively-charged NPs with sizes of 160 nm (A) and 57 nm (B) at 10 mg/L induced mucin (1 mg/L) to aggregate forming large size mucin-NPs aggregates (~6 μm) in 72 hrs ($n \geq 6$). EGTA (2 mM) was added to chelate Ca^{2+} ions that can crosslink mucins forming gels. However, EGTA can not disperse mucin-NPs aggregates after 72 hrs incubation.

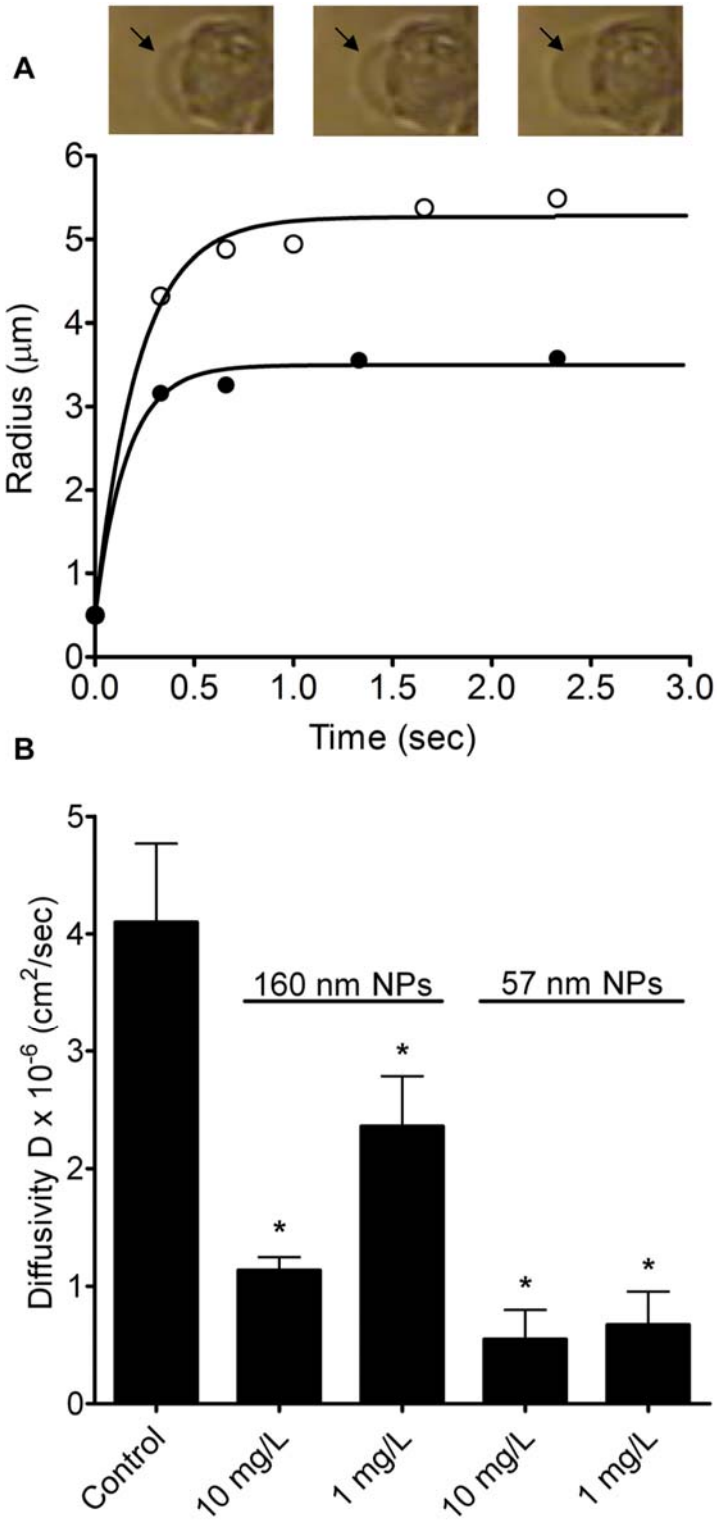
A
Radius (μm)
Time (sec)
B
Diffusivity D x 10-6 (cm2/sec)
160 nm NPs
57 nm NPs
Control
10 mg/L
1 mg/L
10 mg/L
1 mg/L

Figure 4. Effects of NPs on swelling kinetics and diffusivity of secretory granule matrix. (A) Data points of swelling kinetics of secretory granule matrices of A549 cells were fit with equation (1). Exocytosis was triggered by ionomycin. Two representative lines are displayed here. The control (NP free; open circles) shows a higher rate of swelling of newly released mucin network than the swelling rate of mucin matrix when exposed to positively-charged NP (160 nm, 1 mg/L, solid circle). The black arrows indicate the swelling of exocytosed mucin matrix at different time points. (B) Positively-charged NPs hinder the rate of mucin diffusivity (hydration). Mucin post-exocytotic swelling from A549 cells was significantly reduced by positively- charged NPs (160 and 57 nm). This protocol to estimate mucin diffusivity of newly released mucin gels from A549 cells was adapted from our previous study [111]. Data are shown as mean$\pm$SD ($n \geq 10$). NP treated groups are significantly different from the untreated control at $p<0.005$ as indicated by *.

DISCUSSION

Mucus is mainly composed of large and heavily glycosylated glycoproteins called mucin. The gel-forming mucins rapidly hydrate after exocytosis and due to their tangle network properties, anneal with other mucins to form a protective barrier at the airway-surface liquid layer. The mucin gel layer lines the epithelial surface of various organs such as the vaginal tract, eyes, gastric wall and pulmonary lumen [8]. Mucus in the airway of lungs serves as an innate immune defense against inhaled particulates, bacteria and viruses [33]. Maintenance of the airway protection mechanism stems from the delicate balance between normal mucus production, transport and clearance. The mucin polymer network of mucus has a characteristic tangled topology [88]. Since the rheological properties of mucus are governed mainly by the tangle density of mucin polymers, which decreases with the square of the volume of the mucin matrix, the mucin network hydration (degree of swelling) is the most critical factor in determining the rheological properties of mucus [2]. The diffusivity of mucin matrices, which is closely related to mucin viscosity [2,86], can be calculated from polymer swelling kinetics. Based on the polymer network theory, polymer diffusivity is inversely proportional to its viscosity [89,90,91]. Thus, lower rate of mucin diffusivity is associated with higher viscosity, less dispersed and less transportable mucins that appear to characterize the clinical symptoms of thick mucus accumulation and obstruction commonly found in asthma, COPD and CF [16,34,85]. Although chronic exposure to NPs has been shown to induce excessive mucin synthesis [32] and increase the risk of COPD [20], the connection between NPs and poorly dispersed viscous mucus has not been explored.

Due to the versatile application of NPs in nanocarrier delivery systems and commercial products, NPs with varying surface functionalization and characteristics are widely utilized [70,92]. The polyanionic nature of mucin glycoproteins allows for possible electrostatic interactions with oppositely charged NPs. In this study, we investigated how surface charges and size modifications of NPs influence mucus rheological properties. Mucus hydration can be significantly impeded by a change in electrolyte concentration in airway-surface liquid (ASL) [2]. Calcium ion concentration has been shown to increase from 1 mM to 4 mM in the ASL of CF patients, hindering proper mucus swelling and

hydration [93] and leading to respiratory health problems. So far there is no evidence documenting ASL abnormalities in NP-induced airway diseases. However, the mechanism by which NPs can cause changes in the rheological properties of mucus is still unknown.

Gastric mucin was used as a model mucin in our investigation as it shares many similarities with airway mucins [94,95,96]. Our approach is consistent with previous studies that used gastric mucin to examine the viscoelastic properties and biological applications of mucins [97,98,99,100,101,102], since there is currently no commercial mucin sample available that can be preserved in the native state. We utilized DLS to probe the interactions between functionalized NPs and mucin. DLS is a common technique implemented to measure the Brownian motion of mucin polymer in solvent [1,2]. One of the major advantages of this technique is that it enables mucin structure and dynamics to be examined in the native state without chemical fixation, which minimizes protein denaturation and artifacts [1,2]. The diffusion constant that was calculated from Brownian motion measurement is inversely proportional to the hydrodynamic diameter of the measured particle; low diffusion constant usually correlates with large mucin gelation/aggregation [1,2]. As demonstrated by Figures 1A, E & 2A-D, positively-charged NPs can promote mucin aggregation (NP-mucin gel complexes) in a concentration- and size-dependent manner. The mechanism may involve electrostatic attraction between positively-charged NPs and the polyanionic sites on mucin such as the sialic, sulfate and carboxyl functional groups promoting mucin aggregation. By the same notion, mucin polyanionic charges are neutralized by cationic calcium counterions [2] which condenses the mucin matrix and facilitates gel formation [103,104]. On the other hand, negatively-charged and non-functionalized NPs failed to generate significant mucin aggregation. Other studies have shown that hydrophobic and mucin-mucin interactions play vital roles in pH-induced gelation of gastric mucin [105]. However, the hydrophobic moieties on non-functionalized NPs failed to promote significant mucin gelation in our study. This inability might be partially due to the low mucin concentration (1 mg/L) and the neutral pH (buffered at 7.4). The negatively-charged NPs are likely to repel anionic sialic, sulfate and carboxyl functional groups on mucin thereby hindering mucin

aggregation [1,2]. Another possible mechanism could be that these negatively-charged NPs can chelate divalent ions (e.g. Ca^{2+}) in the solution, which play a critical role in mucin gel crosslinking [2].

In addition, our data validated that smaller NPs can induce the formation of larger size mucin aggregated gels more effectively (Figures 1E, 2B & D). The resulting larger mucin gels can possibly be elucidated by differential charge densities on NPs [106]. Our findings are supported by other studies showing that positively-charged chitosan coated NPs, or amine-modified NPs, were highly adhesive to polyanionic mucus gels [107,108]. Viral particles with highly dense positive charges have also been proposed to be more mucoadhesive [8].

After establishing that positively-charged NPs can promote mucin gelation, our data suggests that positively-charged NPs may indeed act as network crosslinkers. Figures 3A & B confirmed that EGTA chelation of indigenous mucin network crosslinker Ca^{2+} ions was unable to disperse the NP-induced mucin aggregation/gelation. Therefore, positively-charged NPs crosslink the polyanionic tangle networks via electrostatic interactions. This evidence further validates the idea that positively-charged NPs effectively replace the natural role of Ca^{2+} ions and highlights the health danger with irreversibly strengthening the crosslinking within mucin gels.

To demonstrate the harmful consequence that positively-charged NPs can have through their crosslinking ability on mucus rheological properties, a swelling kinetics functional assay was used. We determined the direct effect of positively-charged NPs on the mucus hydration rate by measuring the swelling kinetics of newly exocytosed mucin matrices from human lung A549 cells under positively-charged NP exposure. A549 cells are a representative *in vitro* model system for studying mucin swelling kinetics as they express both major respiratory MUC 5AC and MUC 5B mucin proteins [109,110]. Our study showed that positively-charged NPs hindered the rates of mucin matrix hydration and diffusivity in both a concentration- and size-dependent manner (Figures 4A & B). In accordance with the polymer network theory (lower diffusivity correlates with higher

viscosity) [89,90,91], our data indicated that positively-charged NPs decrease the rate of mucin diffusivity and can increase the viscosity of mucin network; the effect of which is further enhanced by smaller sized NPs. Our experimental data has provided the first mechanistic link between positively-charged NPs and altered rheological properties of mucus.

CONCLUSIONS

The positively-charged NPs can crosslink mucins, thus forming NP-mucin gel complexes. The effects of which can potentially induce the formation of viscous mucus and hinder proper mucus hydration and dispersion, leading to impaired mucociliary transport in various epithelial mucosa. The outcome of viscous mucus accumulation could exacerbate pulmonary symptoms of diseased individuals and potentially elevate chances of morbidity in healthy pulmonary systems [17]. As in the case of COPD, CF, or asthma patients, positively-charged NPs could worsen the problem by further thickening the mucus. The complications may include additional reduction in the airway flow or the promotion of chronic bacterial infection. This report also indicates some possible undesirable side effects of drug delivery using positively-charged nanocarriers via epithelial mucosa. These NPs might lead to drug entrapment within mucus, impedance of proper mucus dispersion, and transportability. Our study also found that non-functionalized and negatively-charged NPs have less impact on the rheological properties of mucus. This finding provides the necessary knowledge needed for the safety consideration when using positively-charged functionalized NPs.

CHAPTER 4

A New Role for Bicarbonate in Mucus Formation

ABSTRACT

The impact of small anions on the physical properties of gel-forming mucin has been almost overlooked relative to that of cations. Recently, based on the coincident abnormalities in HCO_3^- secretion and abnormal mucus formed in the hereditary disease, Cystic Fibrosis (CF), HCO_3^- was hypothesized to be critical in the formation of normal mucus by virtue of its ability to sequester Ca^{2+} from condensed mucins being discharged from cells. However, direct evidence of the impact of HCO_3^- on mucus properties is lacking. Herein, we demonstrate for the first time that mucin diffusivity (~1/viscosity) increases as a function of [HCO_3^-]. Direct measurements of exocytosed mucin swelling kinetics from airway cells showed that mucin diffusivity increases by ~300 percent with 20 mM extracellular HCO_3^- concentration. Supporting data indicate that HCO_3^- reduces free Ca^{2+} concentration and decreases the amount of Ca^{2+} that remains associated with mucins. The results demonstrate that HCO_3^- enhances mucin swelling and hydration by reducing Ca^{2+} cross-linking in mucins, thereby decreasing its viscosity and likely increasing its transportability. In addition, HCO_3^- can function as a Ca^{2+} chelator like EGTA (ethylene glycol tetraacetic acid) to disperse mucin aggregates. This study indicates that poor HCO_3^- availability in CF may explain why secreted mucus remains aggregated and more viscous in affected organs. These insights bear not only the fundamental pathogenesis in CF, but also on the process of gel mucus formation and release in general.

Keyword: mucus dispersion, calcium chelation, Cystic Fibrosis and swelling kinetics, mucin viscosity, thickness

INTRODUCTION

Rarely do biology and medicine instruct the physical and chemical sciences, but in this instance a genetic disease may offer new insights into the physical chemistry of forming polymer gels. During gel mucin exocytosis, secreted mucin networks undergo a typical polymer gel phase transition in which the volume may change as much as a 1,000 fold within seconds [2]. Due to the polyanionic nature of the molecular network of mucins, this decondensation of the mucin matrix, driven by a Donnan potential, is considered to be triggered by extracellular Na^+ exchanging for crosslinking Ca^{2+} ions [2,112]. Removing or chelating Ca^{2+} ions results in the rapid swelling, hydration, and dispersion of mucin networks into the extracellular space. Mobile anions in free solution have not been thought to play a significant role in the process. However, Cystic Fibrosis (CF), a life shortening inherited disease of electrolyte transport, suggests a critical role for the free solution anion (HCO_3^-) as a Ca^{2+} chelator in the process of rapid mucin gel swelling [78,113].

The pathogenesis in CF has been well established to result from the formation of abnormal mucus that does not clear properly from the lungs, intestine, and most exocrine glands [114,115]. Various ion transport imbalances have been associated with CF pathology [116,117,118,119,120]. Several cation-centered models (Na^+, Ca^{2+} or H^+) have been proposed to explain the pathogenic mucus [81,93,119,121]. Tangled Ca^{2+}-crosslinked polyanionic polymer networks, like the matrix of mucus, exhibit unique Na^+/Ca^{2+} ion exchange properties that can drastically control mucus swelling equilibrium [88,93,122], and thereby the viscoelastic properties and rheology of the mucus gel [2,89]. Thus, abnormal fluid absorption, failure to reabsorb or chelate Ca^{2+}, and low pH have been proposed to interfere with mucus swelling, leading to defective mucus associated with CF [81,93,119,121].

The most commonly held notion maintains that CF mucus is thick and viscous due to an exaggerated Na^+ dependent fluid absorption that dehydrates secreted mucus [79]. While this effect may seem consistent with manifestations of the disease in the lungs, it is very difficult to extend this rationale to other affected organs where fluid absorption is not

present. Thus, an explanation for the mucus pathology remains perplexing and controversial. Even though HCO_3^- secretion is apparently impaired in organs affected in CF and the severity of the disease seems to correlate with the degree of this impairment [78,113,123,124], the possible involvement of this anion with mucus formation has received little attention [78,113]. Evidence that defective HCO_3^- secretion is associated with abnormal mucus hydration has been recently reported [78,125,126]. Furthermore, activating peroxisome proliferator-activated receptor γ (PPARγ) in CF mice was found to ameliorate the disease by normalizing defects in both HCO_3^- secretion and mucus retention [127]. Thus, defective HCO_3^- secretion could be the possible etiological feature responsible for viscous, unswollen mucus in CF. Nonetheless, evidence that HCO_3^- directly affects mucin swelling and thereby its rheological properties by chelating Ca^{2+} ions has not been experimentally demonstrated until now.

The polymer network of mucus has a characteristic tangled topology [88]. Here we utilized the fact that rheological properties are governed mainly by the tangle density of mucin polymers, which decreases with the square of the volume of the mucin matrix, i.e. the degree of swelling (hydration) critically dictates mucus rheological properties [2]. The diffusivity of mucin matrices, which is closely related to mucin viscosity [2,86,89,90,91,128], can be calculated from polymer swelling kinetics. The rapid swelling of a mucin matrix, such as that which occurs when a mucin granule is secreted and exocytosed, is described with first-order kinetics developed by Tanaka and Fillmore [86]. As shown by previous reports based on polymer physics, polymer diffusivity is inversely proportional to its viscosity [89,90,91,128]. Low mucin diffusivity is associated with higher viscosity, less dispersed, poorly hydrated and probably less transportable mucus that appears to characterize the thick, adhesive accumulations commonly noted in CF [16,85]. We now demonstrate for the first time that HCO_3^- modulates the rheological properties of mucins released from living cells. Our results show that HCO_3^- impedes mucus gel aggregation and increases the diffusivity of exocytosed mucin most likely by chelating Ca^{2+}.

MATERIALS AND METHODS

1. Free calcium measurement

The free calcium measurement was carried out using Ca-selective mini-electrode with a Nernstian response down to a free [Ca^{2+}] of 100 nM or less. The mini-electrodes were prepared as previously described by Schefer [129] and Baudet [130]. In brief, polyethylene tubes were dipped in a membrane solution containing 25 mg ETH-129, 451.5 µl N-phenyl-octyl ether, 12.9 mg potassium tetrakis chlorophenyl borate, and 250 mg polyvinyl chloride, dissolved in 5 ml tetrahydrofuran. The membrane was allowed to air dry, and the filling solution for the electrodes contained 100 mM $CaCl_2$, to give a $1x10^{-1}$ M at pH 7.4. Electrode calibration solutions (CALBUF-1) of 1×10^{-1} M through 1×10^{-8} M were purchased from World Precision Instrument (Sarasota, FL). Normal Hanks' solution (buffered with 20 mM Tris-HCl (Tris(hydroxymethyl)aminomethane hydrochloride) / 10 mM MES (2-(N-Morpholino) ethanesulfonic acid) at pH 7.4) (Sigma, St. Louis, MO) containing 1.2 mM free [Ca^{2+}] was measured as the control. The differences in the mV measured in the control and in subsequent titrations of HCO_3^-, or EGTA (Ethylene glycol-bis(2-aminoethylether)-N,N,N′,N′-tetraacetic acid) (Sigma, St. Louis, MO) (reconstituted in normal Hanks' solution with Tris-HCl/MES pH 7.4), were used to calculate Ca^{2+} concentrations.

To test Cl^- effects on free [Ca^{2+}], PBS (phosphate buffered saline, pH 7.4) based solution containing 1.2 mM Ca^{2+} and 400 mM of Cl^- was serially diluted to various concentrations, ranging from ~ 6 - 400 mM Cl^-, with diluent (1.2 mM $CaCl_2$ and 3 mM KCl, pH 7.4). The differences in mV that were measured in the control (1.2 mM Ca^{2+}) and in serially diluted concentrations of Cl^-, were used to determine Ca^{2+} concentrations.

2. Bound-Ca^{2+} measurement

Bound Ca^{2+} concentration on mucus was measured by inductively coupled plasma optical emission spectrometry (ICP-OES, Perkins-Elmer Optima 5300 DV with concentric nebulizer and cyclonic spray chamber) (Perkins-Elmer, Waltham, MA). 1 mg/L of porcine gastric mucus was prepared by incubating with 4.2 mM of Ca^{2+} containing Hanks' buffer with Tris-HCl/MES at pH 7.4 for 48 hrs. This incubation period allowed

the binding between mucins and Ca^{2+} to reach equilibrium. After 48 hrs, mucins would be crosslinked by Ca^{2+} ions to form mucin aggregates of significant sizes larger than 0.22 μm. This solution was then filtered through a 0.2 μm GTBP Millipore Isopore membrane (Thermo Fisher Scientific, Waltham, MA) to trap the mucin gels. Bicarbonate was then applied to assess its ability to remove mucin-bound Ca^{2+} on Isopore membrane. The Isopore filter was subsequently soaked in 5 ml of 1% HNO_3 (Sigma, St. Louis, MO) to redissolve the trapped mucus with bound Ca^{2+}. The solution was filtered once more using a 0.22 μm Millipore PES membrane (Thermo Fisher Scientific, Waltham, MA). In order to eliminate background interference from the filter-bound Ca^{2+}, an internal control was in place where an Isopore membrane was soaked in 4.2 mM for 48 hrs and the amount of Ca^{2+} deposited in the membrane was measured. This basal value was subsequently subtracted from every treatment to ensure that only mucin-bound Ca^{2+} was quantified.

Calcium in filtrate was detected at wavelengths of 315.893 nm and 317.933 nm. Calcium ICP-MS calibration standards (Thermo Fisher Scientific, Waltham, MA) of 0.05 (1.25 μM), 0.1 (2.5 μM), 1 (25 μM), 10 (250 μM) and 25 (625 μM) mg/L were prepared for the element analyzed and were run at the beginning of the suite. Calcium concentrations were derived from an external standard calibration curve.

An internal control of the total organic carbon in the mucus samples was determined using a Total Organic Carbon Analyzer (TOC-V_{CSH}; Shimadzu, Columbia, MD). The same filtrate used for ICP-OES analysis was first acidified to remove inorganic carbon, such as calcium carbonate and/or bicarbonate, and then diluted 4.2 times with DI water before its measurement for total carbon content. Calibration standards in concentrations of 1, 10 and 50 mgC/L were prepared from the potassium hydrogen phthalate stock standard (Sigma, St. Louis, MO). Carbon contents were measured by TOC-V_{CSH} Analyzer and calculated based on a calibration standard curve. Final results were presented as a molar ratio between bound Ca^{2+} and total mucus organic carbon.

3. Particle sizing

The aggregation of mucus was monitored by measuring particle size by homodyne dynamics laser scattering. Samples of porcine gastric mucus at 1 ng/L were prepared with Hanks' buffer (Tris-HCl/MES, pH 7.4) and were mixed until homogeneity was reached.

Aliquots of mucus solution samples (10 ml) were immediately filtered through a 0.22-μm Millipore PES membrane (pre-washed with 0.1N HCl) into clean scintillating vials to remove dust particles and non-mucin particulates. The scintillating vials were positioned in the goniometer of a Brookhaven laser spectrometer (Brookhaven Instruments, Holtsville, NY). Mucus gel aggregation was allowed to take place by equilibrating with filtered 8.2 mM $CaCl_2$ for 48 hrs and was subsequently analyzed by detecting the scattering fluctuations at a 45 degree scattering angle. Filtered 20 or 50 mM bicarbonate and EGTA (5 mM) solution (buffered with Tris-HCl/MES at pH 7.4) was later added into scintillating vials to test for its ability in dispersing mucus aggregates and was monitored at 1 hr, 2 hrs, 4 hrs, 6 hrs, 16 hrs and 26 hrs. The pH was also monitored and maintained at approximately 7.4 during the experiments. The autocorrelation function of the scattering intensity fluctuations was averaged over a 3-min sampling time using a Brookhaven BI 9000AT autocorrelator. Particle size distribution was calculated by CONTIN [84]. Control experiments were conducted by simultaneously adding 8.2 mM $CaCl_2$ and 20 mM HCO_3^- to 1 ng/L mucus samples (as described above). Mucus aggregation in control samples were monitored throughout 74 hrs. Calibrations were conducted with standard monodisperse suspensions of latex microspheres ranging from 50 nm to 10 μm (Polysciences Inc., Warrington, PA).

4. Mucus aggregation

HCO_3^- was tested for its effect on reducing the amount of mucus aggregates. Porcine gastric mucus (5 μg/mL) was used as a model for gel forming mucus. The dried mucus was added with 13 mM $Ca(OH)_2$ to distilled water and agitated overnight until the mucus powder dissolved. This solution was divided into equal volumes of two aliquots; 100 mM NaCl was added to one while 100 mM $NaHCO_3$ (Sigma, St.Louis, MO) was added to the other; both were stirred for 3 hrs. Each mucus solution was filtered through an immobilon-P transfer membrane (IPVH00010, Millipore, Billerica, MA; filter pore size: 0.45 μm). The membrane filters were dried in a vacuum oven and weighed before and after filtration. The difference in weights of the dried membrane filter before and after filtering defined the amount of aggregated mucus retained on the filter. The amount of retained mucus was normalized to the volume of mucus solution filtered.

5. A549 cell culture

The human lung carcinoma cell line A549 was obtained from American Type Culture Collection (ATCC, Manassas, VA). The A549 cell line is an airway alveolar epithelial cell line commonly used as a secretory model [83]. Cells were cultured in 15 cm cell culture plates (VWR, Brisbane, CA) containing F-12 nutrient mixture medium (Invitrogen, Carlsbad, CA) supplemented with 100 U of penicillin/streptomycin (Invitrogen, Carlsbad, CA) and 10% heat-inactivated fetal bovine serum (FBS) (Invitrogen, Carlsbad, CA). The A549 lung cells were cultured in 15 cm falcon plates and incubated in a humidified incubator at 37℃/5% CO_2. Cell counts were performed using trypan blue (Sigma, St. Louis, MO) exclusion and a Bright-Line haemocytometer.

6. Secretory granule labeling

The presence of secretory granules of A549 cells was identified by staining with quinacrine (10 μM; Sigma, St. Louis, MO) for 15 min. The nucleus was counterstained with Hoechst (1:1000, Sigma, St. Louis, MO) followed by thorough rinsing and mounting of the sample. Expression of MUC5AC in A549 cells was confirmed by immunostaining (data not shown).

7. Swelling kinetics and A549 cell preparation

The culture plates were rinsed with Hanks' buffer twice. Non-trypsin dissociation buffer (Invitrogen, Carlsbad, CA) was added to detach cells from plates and subsequently incubated at 37° C for 15 min, centrifuged at 700 rpm for 5 min, and resuspended in Hanks' buffer (Invitrogen, Carlsbad, CA). Resuspended cells were dispersed into MatTek glass bottom dishes (MatTek Corporation, Ashland, MA) and equilibrated in a 37°C incubator for 10 min prior to adding varying concentrations of HCO_3^- or EGTA. Both Hanks' solution and HCO_3^- solutions were buffered with Tris-HCl and MES (Sigma, St. Louis, MO) to pH 7.4. The pH was monitored and maintained at approximately 7.4 throughout the experiments.

A549 cells were viewed and video-recorded with phase-contrast lens using a Nikon Eclipse TE-2000-U inverted fluorescence microscope (Nikon Eclipse TE-2000U, Tokyo, Japan). Degranulation of A549 was induced by 1 μM ionomycin (Sigma, St. Louis, MO) and was found to be a readily observable discrete quantal process. During exocytosis into extracellular Hanks' solution, released granules undergo rapid swelling. Video-recordings of granular exocytosis and swelling were captured at 30 frames s^{-1}. The analysis of the changing mucin matrix dimension was assessed with NIS-Elements software (Nikon, Melville, New York).

Measurements of the radii of the released mucus matrices, as a function of time, were used to verify that the swelling of the secreted material followed the characteristic features of polymer gel swelling kinetics [85,86]. The swelling of a polymer follows a typical diffusive kinetics that is independent of the size, internal topology, or chemical composition of the gel [86]. For spherical gels, as observed with the exocytosed mucin granules of A549 cells, the radial dimension increases following a characteristic first order kinetics of the form $r(t) = r_f - (r_f - r_i)\, e^{-t/\tau}$, where r_i and r_f are the initial and final radii of the granule matrix, respectively, and τ is the characteristic relaxation time of the swelling process [2]. The polymer network of gels diffuses into the solvent (Hanks' solution), with diffusivity (D) ($D = (r_f)^2/\tau$ [$cm^2\ s^{-1}$]). The diffusivity (D) of polyionic gels varies with the concentration of counterions in the swelling medium. In this study, we measured the swelling kinetics of exocytosed mucin gels in Hanks' buffer (Invitrogen, Carlsbad, CA) with HCO_3^- concentrations in the physiological range of 0-140 mM. Previous reports have predicted that polymer viscosity is proportional to the molecular weight of polymers and that polymer diffusivity is inversely proportional to the molecular weight. Therefore, polymer viscosity and diffusivity are inversely proportional to each other [89,90,91,128]. Higher polymer diffusivity indicates lower viscosity of polymers. Thus, we can take direct measurements of changes in mucin diffusivity under different HCO_3^- concentrations as changes in mucin viscosity.

8. Statistical analysis

Data was presented as means $\pm$ SD. Each experiment was performed independently at least three times. Statistical significance was determined using a Student's t-test analysis with p values of <0.05 (Microsoft Excel and GraphPad Prism 4.0, GraphPad Software, Inc., San Diego, CA).

RESULTS

HCO_3^- lowers free Ca^{2+} concentration by chelating Ca^{2+}

We directly measured the concentration of free Ca^{2+} in Hanks' solution (1.2 mM Ca^{2+}) with a Ca^{2+}-selective mini-electrode in increasing concentrations of HCO_3^-. As [HCO_3^-] increased from 0 - 50 mM, the concentration of free Ca^{2+} decreased exponentially from 1.2 mM to < 50 μM (Fig. 1A), with most of the reduction occurring at < 5 mM HCO_3^-. As [HCO_3^-] approaches 10 mM, the decrease in free [Ca^{2+}] starts to plateau so that there was little change with 20 - 50 mM HCO_3^-. These results demonstrate that HCO_3^- removes most free Ca^{2+} from Hanks' buffer solutions at relatively low concentrations (extracellular HCO_3^- concentration is normally ~24 mM). As a positive control, increasing concentrations of EGTA (1 - 5 mM) resulted in a subsequent decrease of free [Ca^{2+}] from 1.2 mM to almost 0 mM in normal Hanks' solution (Fig. 1A inset). To confirm that Cl^-, the most common physiologically abundant extracellular anion (normally ~110 mM), does not chelate free Ca^{2+} ions, we increased total [Cl^-] up to 400 mM and found that the level of free [Ca^{2+}] in Hanks' buffer was not altered (Fig. 1B).

HCO_3^- chelates mucus-bound Ca^{2+}

To investigate whether HCO_3^- ions are also able to chelate mucus-bound Ca^{2+}, inductively coupled plasma optical emission spectrometry (ICP-OES) was used to quantify the relative amount of bound Ca^{2+} displaced from mucus after adding 20 mM HCO_3^- at increasing intervals of time. Mucus (1 mg/L) was prepared in Hanks' solution (buffered with Tris-HCl/MES at pH 7.4) containing 4.2 mM Ca^{2+} since [Ca^{2+}] found in CF mucus is approximately 2 - 4 mM [93]. The mucus solution was combined with 20 mM HCO_3^- and assayed at 0, 5, 15 and 30 minutes (Fig. 2). No significant amount of $CaCO_3$ precipitation (> 200 nm) was observed during the sample preparation (data not shown). The mucus sample was filtered through a 0.2 μm Isopore membrane and redissolved in 1% HNO_3 solution. The data shows that as HCO_3^- incubation time increases, the amount of mucus-bound Ca^{2+} decreases (Fig. 2). Within five minutes of HCO_3^- exposure, bound Ca^{2+} dramatically dropped to 56% and continued to fall to 28%

of the control after 30 minutes of incubation with HCO_3^-. These results show that HCO_3^- readily sequesters bound Ca^{2+} from mucus.

HCO_3^- disperses aggregated mucus

We then undertook showing that HCO_3^- can directly disperse aggregated mucus gels (Fig. 3). Porcine gastric mucus (1 ng/L) was added with 8.2 mM Ca^{2+} in Hanks' solution (buffered with Tris-HCl/MES at pH 7.4) and was equilibrated for at least 48 hrs until significant aggregation of mucus masses of approximately 9 μm in diameter was attained. The 8.2 mM Ca^{2+} was used to gelate dilute mucus for studying the dispersion capacity of HCO_3^-. Upon addition of 20 or 50 mM HCO_3^- (buffered with Tris-HCl/MES at pH 7.4), aggregated mucus gel particles dispersed and decreased in size from ~9 μm to ~4.5 μm (Fig. 3). A time-dependent decrease in mucus gel size reached an apparent minimum in about 6 hrs. Addition of EGTA (Ca^{2+} chelator, 5 mM) also dispersed aggregated mucus gels to approximately the same size. Aggregated mucus gel size did not return to its original size (~0.2 μm) with either HCO_3^- or EGTA treatment (Fig. 3). This data indicates that HCO_3^- likely disperses Ca^{2+} crosslinked mucus gels [78] by sequestering free and bound Ca^{2+} ions from mucus networks as well as from free solutions.

The result shown in Figure 4 demonstrates on a gross level that HCO_3^- reduces apparent mucus aggregates. After filtering gastric mucus through a 0.45 μm pore immobilon-P transfer membrane in the presence of $NaHCO_3$ (100 mM), only 0.27 mg/ml was retained. However, in the presence of NaCl (100 mM) twice as much filtered mucus gel (0.56 mg/ml) was retained. This direct measurement of aggregated mucus confirms that HCO_3^- disperses aggregated mucus and that Cl^- ions have little, if any, effect on mucus aggregation.

HCO_3^- accelerates mucin matrix expansion

A representative plot comparing the swelling kinetics of newly exocytosed mucin matrices between the control (HCO_3^- free) and HCO_3^- treatment is shown in Figure 5A. The rate of mucin network swelling (hydration) was significantly elevated in the presence of HCO_3^- (Fig. 5A). Converting swelling rate into diffusivity (D) yielded similar results

(Fig. 6). Digital images capturing the process of mucin matrix gel swelling were also presented (Fig. 5B). In addition, through the use of fluorescent dye, quinacrine, we confirmed the presence of mucin granules in A549 cells [19,131] (Fig. 5C). The fluorescent secretory granules (green) distributed in the cytosol surrounding the nucleus, which stained with Hoechst dye (blue).

HCO_3^- markedly enhances secreted mucin diffusivity

Exocytosis of mucin granules from cultured A549 cells was stimulated with 1 μM ionomycin [18] and mucin diffusivity was calculated from the swelling kinetics as described (see methods) [85]. A faster mucin gel swelling rate indicates greater mucin diffusivity and a less viscous gel [85]. Mucin matrix swelling rates were accelerated by increasing bicarbonate concentrations (0-140 mM, Fig. 6). The increase in mucin swelling rate was HCO_3^- concentration dependent. Compared to controls in HCO_3^- free Hanks' medium, in 1 mM HCO_3^-, there is a 160% increase in mucin diffusivity while at 10 mM HCO_3^-, diffusivity was increased by 190%. Diffusivity further increased to 280% at 20 mM HCO_3^- and to 540% at 140 mM HCO_3^-, relative to the control (no bicarbonate). The concentration range of HCO_3^- applied was based on physiological concentrations [132,133]. Moreover, EGTA (5 and 10 mM) was used as a positive control for Ca^{2+} chelation, which increased diffusivity by 190% and 360% (open circles) (Fig. 6). These results confirm that HCO_3^- at physiological concentrations dramatically decreases mucin viscosity by sequestering Ca^{2+}.

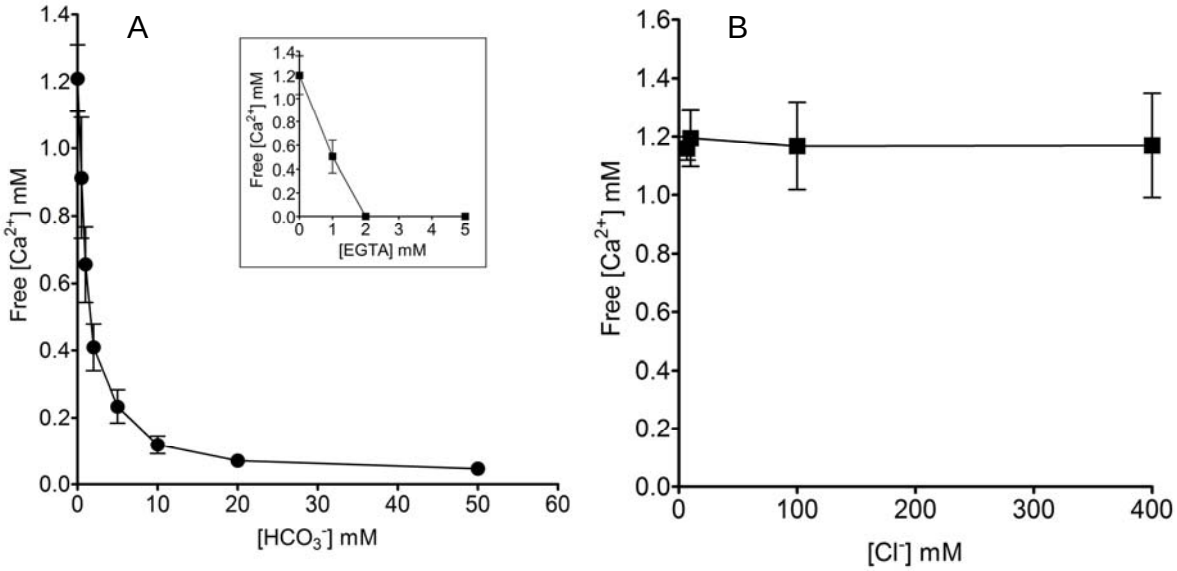

Figure 1. Bicarbonate reduces the free Ca^{2+} ion concentration. A) Incremental increases in HCO_3^-concentration apparently reduce free Ca^{2+} from Hanks' medium (1.2 mM Ca^{2+}). The data show 1) that free Ca^{2+} in normal isotonic extracellular media in the presence of physiological concentrations of HCO_3^- should be less than 0.1 mM, and 2) that the high concentrations of Ca^{2+} in the condensed mucin of exocytosed granules likely could be chelated by HCO_3^-/CO_3^{2-} in the media. EGTA, used as a positive control, also decreases the level of free Ca^{2+} in normal Hanks' medium (1.2 mM Ca^{2+}; see inset). Each point corresponds to the mean ± SD ($N \geq 6$). B) Chloride ions have no effect on the free Ca^{2+} ion concentration in PBS solution. Each point corresponds to the mean ± SD ($N = 5$).

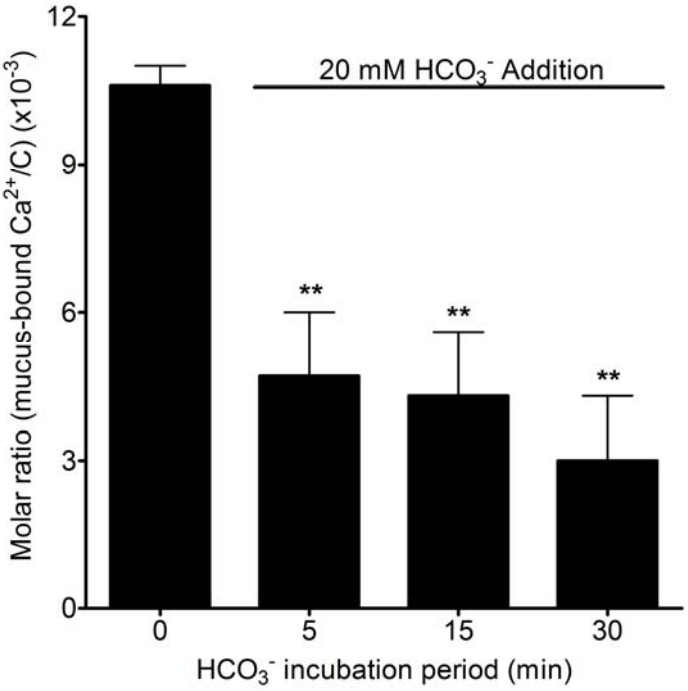

Figure 2. Bicarbonate can chelate the bound Ca^{2+} ions from mucus gels. Each data point corresponds to the mean ± SD ($N \geq 8$). All bicarbonate treated groups are significantly different from the control (bicarbonate free) (**$P < 0.005$). The amount of bound Ca^{2+} ions was determined with inductively coupled plasma optical emission spectrometry (ICP-OES) and the total organic carbon was measured with a Total Organic Carbon Analyzer (TOC-V_{CSH}; Shimadzu).

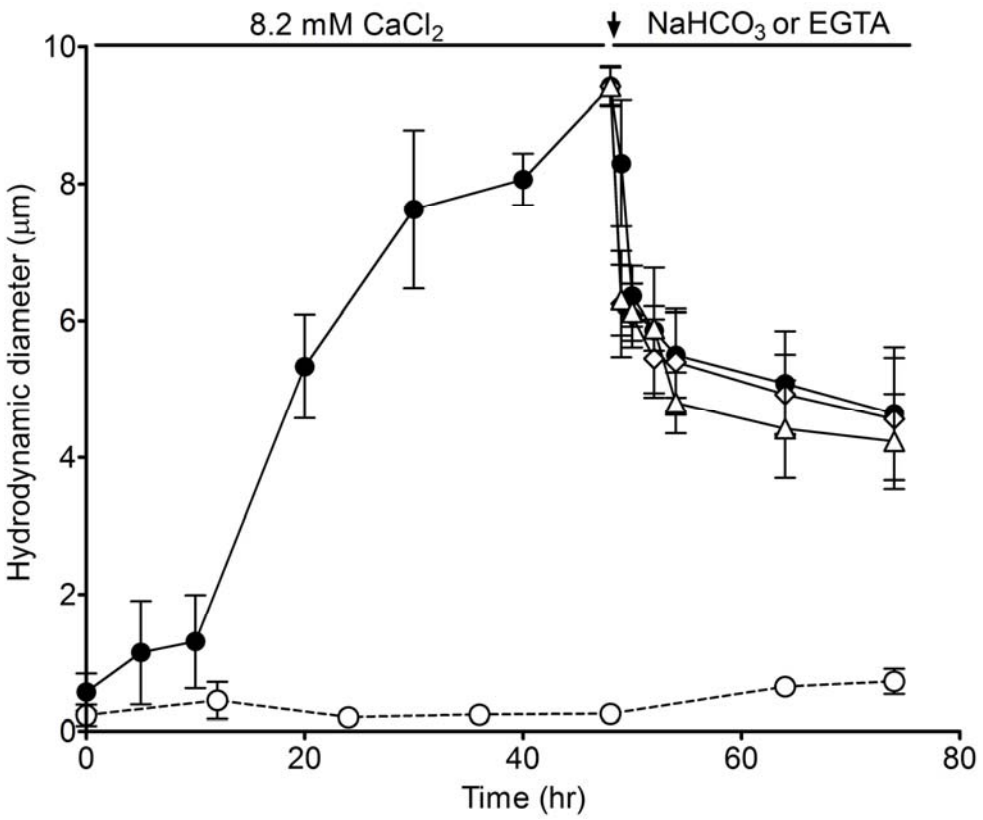

Figure 3. Bicarbonate (20 mM and 50 mM) disperses aggregated mucus gels monitored with dynamic laser scattering. The average size of mucin gels at Ca^{2+} = 8.2 mM (solid circles, N $\geq$ 4) increased to approximately 9.4 μm within the initial 48 hrs of incubation and decreased upon bicarbonate application (20 mM, solid circles, N $\geq$ 6; 50 mM, open diamonds, N $\geq$ 6). Addition of EGTA (positive control) also dispersed aggregated mucus gels (5 mM, open triangles, N $\geq$ 7). The control sizes remained low (open circles, N $\geq$ 3) when compared with treatment groups.

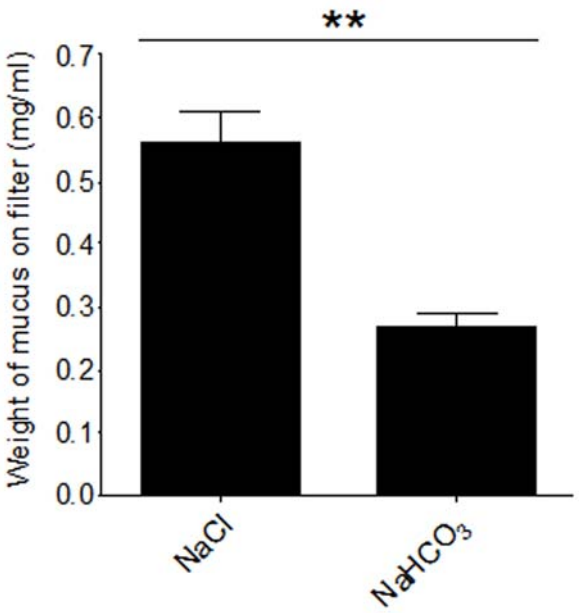

Figure 4. Mucus powders solubilized in 100 mM Cl^- or HCO_3^-. The amount of filtered mucus retained on filters (0.45 μm) was more than double for the Cl^- solution (0.56 mg/ml) than for the HCO_3^- solution (0.27 mg/ml) (** $P < 0.005$).

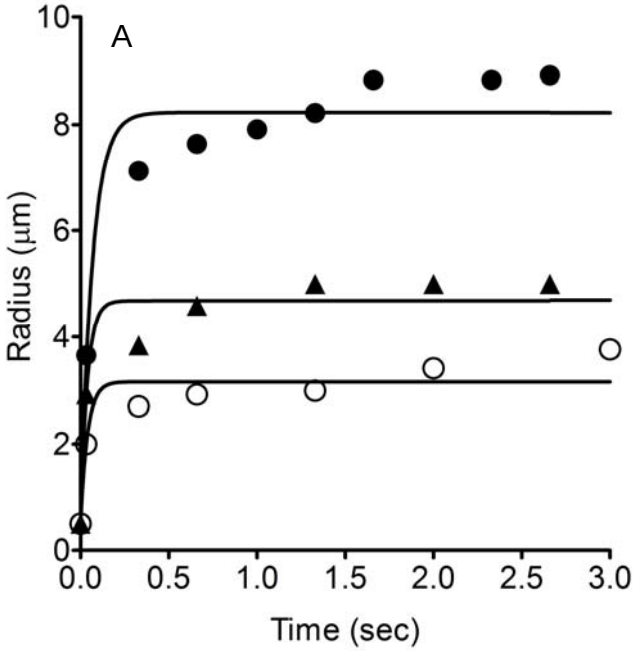
A
10
8
6
4
2
0
Radius (µm)
0.0
0.5
1.0
1.5
2.0
2.5
3.0
Time (sec)

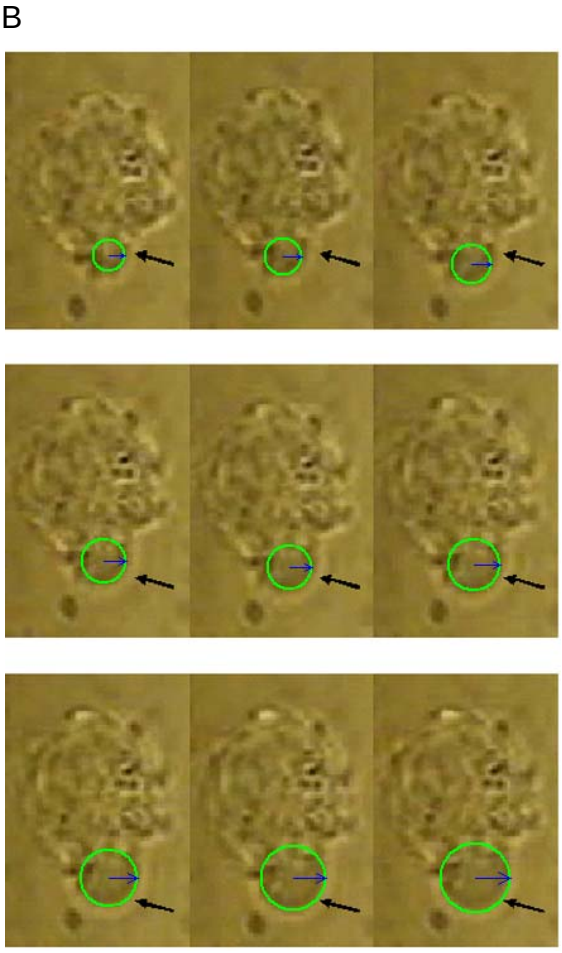
B

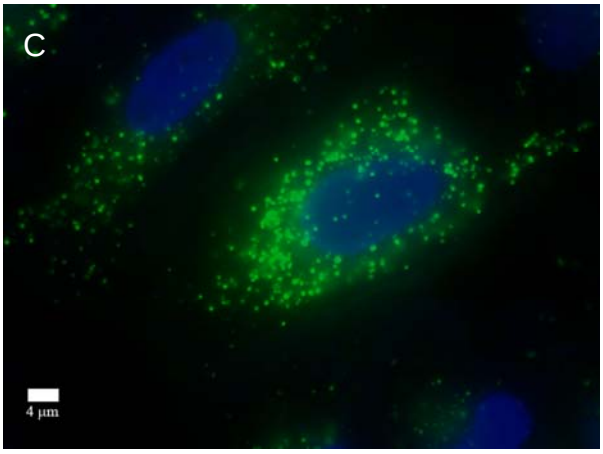
C
4 µm

Figure 5. Identification of secretory granules and measurement of mucin matrix expansion. A) A representative plot of the swelling kinetics (hydration) of mucin matrices secreted by A549 cells is shown. The data points were fitted with the characteristic first order kinetics equation (see methods). The control (bicarbonate free, open circles) shows a lower rate of mucin matrix swelling when compared with the swelling rate during bicarbonate exposure (140 mM HCO_3^-, solid circles; 20 mM HCO_3^-, solid triangles). B) Digital images demonstrating mucin matrix expansion during exocytosis, recorded by videomicroscopy are presented. Exocytosis was triggered by ionomycin. The arrows indicate the expanding mucin granule matrix whose radii are automatically measured by green circles generated by NIS-Elements (Nikon, Melville, New York). C) Loading of quinacrine dye showed the presence of green secretory granules in the cytosol of A549 cells. The nucleus was stained blue with Hoechst dye.

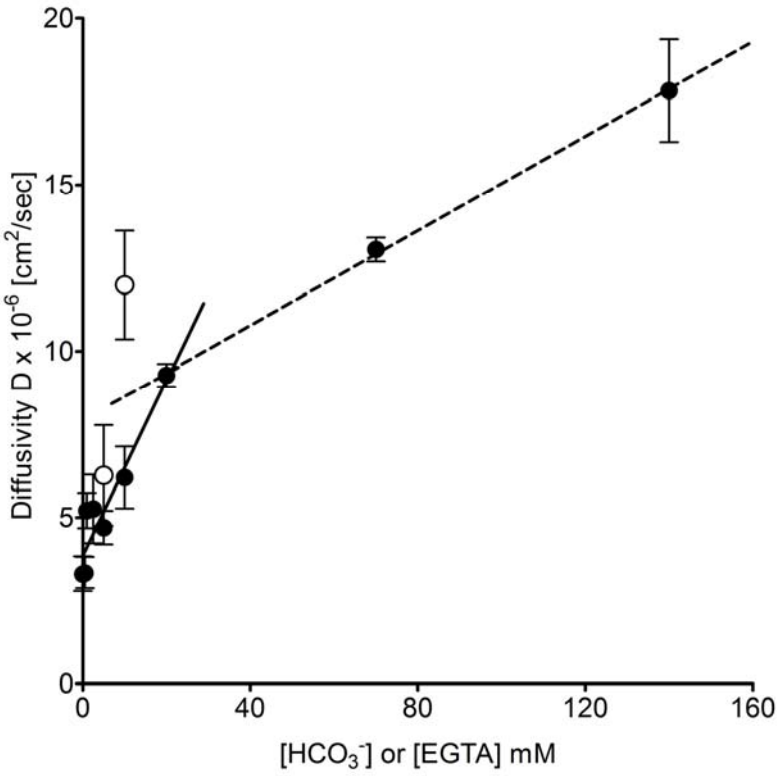

Figure 6. Bicarbonate increases mucin diffusivity secreted from A549 cells. The increase of diffusivity suggests that HCO_3^- may chelate Ca^{2+} from two different pools (solid circles). EGTA (5 and 10 mM, open circles) also markedly increased the diffusivity and is shown as open circles. Each point corresponds to the mean ± SD ($N \geq 6$).

DISCUSSION

The formation of mucus is one of the most complex processes of physical chemistry in biology; fundamentally, it is accepted that before being secreted, highly negatively charged mucin polymer matrices are tightly packed within granules at a low pH in a very high concentration of intragranular Ca^{2+} [2]. The negative charges of the mucin matrices are shielded and neutralized by protons and electrostatic divalent Ca^{2+} cross-links. In order to maintain proper and normal luminal and ductal transport of released mucin, adequate swelling and hydration of gel matrices are essential [2,16]. In order for the electrostatic forces to expand the matrix, the mucin anions must be unshielded and the inter- and intramolecular cross-links removed. Until now, it has been generally accepted that the swelling process depends essentially upon exchanging monovalent cations (Na^+ and K^+) in the medium for protons and divalent Ca^{2+} in the matrices; however, recent recognition that the abnormally viscous mucus consistently found in CF may be the result of the absence of HCO_3^- in this disease (31) seems to provide additional insight into the physical/chemical process of mucus formation. Moreover, the chemical properties of HCO_3^-, per se, also suggest that among biological ions, it is ideally suited to support Ca^{2+} removal. That is, the poor solubility of $CaCO_3$ ($K_{sp} = 4.8\times10^{-9}$) indicates strong binding between Ca^{2+} and CO_3^{2-} ions [134], and the equilibrium between HCO_3^- and CO_3^{2-} support multiple complexes with Ca^{2+} ions [78,135].

To confirm that bicarbonate sequesters Ca^{2+} at physiological fluid concentations, we measured free Ca^{2+} concentration in Hanks' solution after adding HCO_3^- and found that a steep drop in free Ca^{2+} occurred with low mM HCO_3^- concentrations (Fig. 1A) due to forming Ca^{2+} complexes, e.g. $CaCO_3$ and $CaHCO_3^+$ [135]. Further decreases in free Ca^{2+} were negligible even in the presence of higher HCO_3^- concentration (50 mM), indicating that nearly all Ca^{2+} available in solution can be sequestered by HCO_3^- concentrations that are easily achieved physiologically. The other major physiological anion, Cl^-, had no effect on free Ca^{2+} as $CaCl_2$ remains essentially dissociated in the HCO_3^- free solution (Fig. 1B). To be effective in mucus expansion, HCO_3^- must not only remove free solution Ca^{2+}, but it must also remove calcium bound in the mucin matrix. We used a commercial

source of mucus, which is not pure mucin, but may serve to represent mucus gel interactions. This approach is consistent with previous studies using this porcine gastric mucin to examine the viscoelastic properties and biological applications of mucin [97,99,100,102]. There is currently no commercial mucin sample available that has been perfectly preserved in the native state. After equilibrating with Ca^{2+}, we found that adding 20 mM HCO_3^- to the mucus solution removed more than half the bound Ca^{2+} within a few minutes and about three fourths within 30 minutes (Fig. 2). Thus, HCO_3^- is capable of chelating free Ca^{2+} from solution and sequestering bound Ca^{2+} from mucus gel matrices.

We then asked whether sequestering Ca^{2+} with HCO_3^- could enhance the dispersal of aggregated mucus. Both 20 and 50 mM of HCO_3^- dispersed aggregated mucus gels and almost immediately reduced the size of consolidated aggregates by 50% (Fig. 3), but further disaggregation did not occur. Chelation of Ca^{2+} has been reported to disperse polymer gels [84]. Adding EGTA, a highly efficient Ca^{2+} chelator, in place of HCO_3^-, dispersed aggregated mucus very similarly (Fig. 3). This result probably indicates the importance of Ca^{2+} crosslinking in mucin aggregation and accumulation. However, the fact that EGTA produced the results similar to HCO_3^- indicates that the failure to completely reverse the disaggregation is not due to incomplete sequestration of Ca^{2+} by HCO_3^- and may not be entirely due Ca^{2+}. Additional hydrophobic interactions may also be present within aggregated mucus [1,105]. The data in Figure 4 corroborates these findings by showing that compared to Cl^-, HCO_3^- greatly reduced the amount of aggregated mucus gels retained on a micro filter (Fig. 4).

These combined results demonstrate that HCO_3^- can play a critical role in the decondensation of mucin granules, but proof awaits a direct demonstration of its effects on mucus properties *in vivo*. Hydration-induced swelling is the single most critical determinant of mucus rheological characteristics [2,85,136] and measurements of mucin swelling kinetics (diffusivity) provides a unique method to directly assess changes in mucin rheological properties (viscosity) released from living cells under physiological conditions [2,136]. A549 cells were used as our representative model system for studying

mucin swelling kinetics because it produces both major respiratory MUC5AC and MUC5B gel forming mucins [109,110]. Therefore, using videomicroscopy of living A549 cells in culture, we measured the rates of swelling in real time of mucin granules released from cells that were stimulated to secrete into different concentrations of HCO_3^-. First, our data showed that at physiological HCO_3^- concentrations, a mucin network rapidly hydrates (Fig. 5A), which we surmise would render it more easily transportable. Second, a biphasic response of mucin swelling rates to increasing bicarbonate concentrations is clearly demonstrated in Figure 6. The two different slopes may suggest the existence of two different Ca^{2+} binding sites within mucins. This second phase might reflect removal of a more tightly bound source of Ca^{2+} in the mucin. That is, at lower HCO_3^- concentrations, the swelling may be dominated by repulsion of the highly anionic, highly-glycosylated regions of the mucin freed upon removing Ca^{2+} cross-linking as fixed negative charges are unshielded [78,137,138]. Higher concentrations of HCO_3^- (and associated CO_3^{2-}) might be competing tightly bound Ca^{2+} away from other binding sites, such as those recently described as nodes of tightly bound protein domains in mucins [137,138]. Chelating Ca^{2+} with EGTA (5 and 10 mM) confirmed the notion that the increased rate of diffusivity is due to Ca^{2+} removal. EGTA (5 and 10 mM) sequestration of Ca^{2+} increased the mucin network diffusivity by 190% and 360% compared to the control (no EGTA) while 5 mM, 20 mM and 140 mM HCO_3^- increased diffusivity by 140%, 280% and 540% compared to the control (HCO_3^- free) (Fig. 6). Based on concentration, EGTA seems to be somewhat more effective than HCO_3^- likely due to the stronger chelation affinity of EGTA for Ca^{2+}. These data provide the first direct experimental evidence that HCO_3^- modulates the mucin hydration rate and the viscoelastic properties (viscosity) of mucins in live cells.

Since the medium concentrations of Na^+ and K^+ were constant in all protocols, the increases in diffusivity cannot be due solely to the exchange of calcium with Na^+ or K^+ ions. The same consideration can be made in Cystic Fibrosis where the concentration of these monovalent cations is relatively normal and constant, but it is the HCO_3^- that is diminished. Clearly Na^+/Ca^{2+} exchange must occur to maintain electroneutrality within the matrix. However, HCO_3^- may be necessary to speed or facilitate the exchange by

"competing" Ca^{2+} away from fixed anions on the mucin molecules so that the monovalent cations (Na^{+}) can replace the Ca^{2+} that would otherwise remain bound, and slow or impossible to remove solely by cation exchange. This would almost certainly be the case if fixed mucin anions have a higher affinity for Ca^{2+} than for Na^{+}.

With respect to Cystic Fibrosis, which instigated this study, previous work recently demonstrated that the amount of mucus discharged from the intestine [139] and the uterine cervix [126] *in vitro* was significantly reduced when HCO_3^- secretion was impeded. The present work provides a likely basis for those findings and possibly for the characteristically aggregated and tenacious mucus abnormalities found in Cystic Fibrosis as well. That is, in CF where the genetic defect occurs in a gene that codes for an anion channel, it is now well established that, like Cl^-, HCO_3^- permeability and secretion are greatly reduced or absent [78,113]. Our studies here strongly indicate that in CF organs, when mucins are released into fluids without adequate HCO_3^-, their diffusivity would be decreased (viscosity increased); normal expansion of mucins would be retarded and impaired due to retained Ca^{2+} crosslinking, and the long observed pathogenic aggregation and stagnation of "sticky" mucus would tend to occur. A tentative model of this process was proposed recently [126]. It should be noted that organ failure in CF is not immediate and generally occurs over many months or years, so that pathogenic mucus aggregation is almost surely a multifactorial process.

In summary, we have demonstrated that HCO_3^- ions play a critical role in determining the viscosity of mucins and mucus by controlling swelling and dispersion most likely by competing with fixed anions in mucins for Ca^{2+}, which condenses and aggregates mucus polymers via divalent crosslinking. These findings show that defects in bicarbonate ion transport such as those associated with CF can lead to pathologically thick and viscid mucus for which CF is known. These results may provide insights for new therapeutic strategies to reduce organ failure in CF due to mucus obstructions and to ameliorate problems in other diseases of mucus.

CHAPTER 5

Conclusion and future directions

The aims of my Ph.D. projects investigated how physiological and environmental factors modulate (i) mucin secretion and (ii) viscoelasticity which are vital to pulmonary health. NP exposure, in the forms of airborne particulates and pollutants, has shown to exert harmful effects on pulmonary cellular physiology. It was documented that geographical areas heavily polluted with NPs also exhibited significantly elevated incidences of pulmonary diseases such as asthma and COPD and exacerbated respiratory symptoms particularly thick mucus obstruction [25, 52]. TiO_2 NPs are commonly applied in the nanoindustry and pervasively used in daily products. However, studies that investigate the harmful capacity of TiO_2 NPs to directly induce mucin secretion from airway epithelial cells are scarce. Moreover, it is not clear whether functionalized NP and anions play critical roles in determining the rheological properties of mucus during health and disease.

In TiO_2 NP-induced mucin secretion from airway epithelial cells, our major findings were that TiO_2 NPs could elicit an intracellular Ca^{2+} signaling associated secretion. TiO_2 NPs either triggered an activation of L-type Ca^{2+} channel or perturbed membrane integrity which led to an influx of extracellular Ca^{2+}. This process may be mediated by the synthesis of ROS since addition of NAC significantly attenuated the intracellular Ca^{2+} rise. Elevated cytosolic Ca^{2+} levels then triggered a secondary Ca^{2+} amplification involving ryanodine receptor-linked CICR mechanism. Blocking ryanodine receptors significantly reduced the sustained cytosolic Ca^{2+} rise and abolished the subsequent secretory response. Our data suggests that pharmacological blockers or anti-oxidant treatments down-regulating the Ca^{2+} relay system and the generation of ROS could become potential drugs targeting abnormal mucin hypersecretion. Future studies involving pulmonary disease animal models will further confirm the hypothesis. Moreover, it has been shown that mucin protein synthesis is up-regulated in animal models exposed to NP insults [29]. Besides focusing on the secretory response,

understanding the cellular mechanisms behind mucin hyper-production and possible contribution from neural stimulation will provide insights to future therapeutic strategies.

In functionalized NP-induced changes in mucin viscoelasticity, our results showed that positively-charged functionalized NPs crosslinked mucin gels, reduced mucin hydration rate and increased mucin viscosity. Whereas bicarbonate ions served as Ca^{2+} chelators which reduced both free Ca^{2+} in solution and mucin-bound Ca^{2+}, and accelerated mucin diffusivity. Consequently, mucin becomes less viscous, more transportable and properly hydrated. Our data demonstrated a possible mechanistic link between NP exposure and thick mucus that occludes airway lumen observed in patients with respiratory diseases. More importantly, our results elucidate why a defective CFTR anionic channel, which also impairs bicarbonate transport, can associate with clinical symptoms of viscous mucus plugs in cystic fibrosis sufferers. As a future therapy for dispersing airway mucus, bicarbonate or chemicals with a Ca^{2+} chelating ability may play a critical role. Clinical trials may be needed to authenticate the feasibility and the potential to apply to treat complications in different organ systems.

REFERENCES

1. Bansil R, Stanley E, J.T. L (1995) Mucin Biophysics. Ann Rev Physiol 57: 635-657.
2. Verdugo P (1990) Goblet cells secretion and mucogenesis. Ann Rev Physiol 52: 157-176.
3. Fahy JV, Dickey BF (2010) Airway mucus function and dysfunction. N Engl J Med 363: 2233-2247.
4. Rose MC, Voynow JA (2006) Respiratory tract mucin genes and mucin glycoproteins in health and disease. Physiol Rev 86: 245-278.
5. Tesfaigzi Y (2008) Regulation of mucous cell metaplasia in bronchial asthma. Curr Mol Med 8: 408-415.
6. Thornton DJ, Rousseau K, McGuckin MA (2008) Structure and function of the polymeric mucins in airways mucus. Annual Review of Physiology 70: 459-486.
7. Zhu Y, Ehre C, Abdullah LH, Sheehan JK, Roy M, et al. (2008) Munc13-2-/- baseline secretion defect reveals source of oligomeric mucins in mouse airways. J Physiol 586: 1977-1992.
8. Cone RA (2009) Barrier properties of mucus. Adv Drug Deliv Rev 61: 75-85.
9. Lai SK, Wang YY, Wirtz D, Hanes J (2009) Micro- and macrorheology of mucus. Adv Drug Deliv Rev 61: 86-100.
10. Thornton DJ, Sheehan JK (2004) From mucins to mucus: toward a more coherent understanding of this essential barrier. Proc Am Thorac Soc 1: 54-61.
11. Kesimer M, Kirkham S, Pickles RJ, Henderson AG, Alexis NE, et al. (2009) Tracheobronchial air-liquid interface cell culture: a model for innate mucosal defense of the upper airways? Am J Physiol Lung Cell Mol Physiol 296: L92-L100.
12. Chen EY, Garnica M, Wang YC, Chen CS, Chin WC (2010) Mucin Secretion Induced by Titanium Dioxide Nanoparticles PLoS One: In press.
13. Chen EY, Wang YC, Chen CS, Chin WC (2010) Functionalized Positive Nanoparticles Reduce Mucin Swelling and Dispersion. PLoS One 5: e15434.
14. Chen EY, Yang N, Quinton PM, Chin WC (2010) A New Role for Bicarbonate in Mucus Formation. Am J Physiol Lung Cell Mol Physiol 299: L542-549.
15. Rogers DF, Barnes PJ (2006) Treatment of airway mucus hypersecretion. Annals of Medicine 38: 116-125.
16. Randell SH, Boucher RC, Grp UNCVL (2006) Effective mucus clearance is essential for respiratory health. Am J Respir Cell Mol Biol 35: 20-28.
17. Hogg JC, Chu F, Utokaparch S, Woods R, Elliott WM, et al. (2004) The nature of small-airway obstruction in chronic obstructive pulmonary disease. N Engl J Med 350: 2645-2653.
18. Abdullah LH, Conway JD, Cohn JA, Davis CW (1997) Protein kinase C and Ca2+ activation of mucin secretion in airway goblet cells. Am J Physiol 273: L201-210.
19. Nguyen T, Chin WC, Verdugo P (1998) Role of Ca2+/K+ ion exchange in intracellular storage and release of Ca2+. Nature 395: 908-912.
20. Alfaro-Moreno E, Nawrot TS, Nemmar A, Nemery B (2007) Particulate matter in the environment: pulmonary and cardiovascular effects. Curr Opin Pulm Med 13: 98-106.

21. Gwinn MR, Vallyathan V (2006) Nanoparticles: health effects--pros and cons. Environ Health Perspect 114: 1818-1825.
22. Sethi S (2004) New developments in the pathogenesis of acute exacerbations of chronic obstructive pulmonary disease. Curr Opin Infect Dis 17: 113-119.
23. Atkinson RW, Anderson HR, Sunyer J, Ayres J, Baccini M, et al. (2001) Acute effects of particulate air pollution on respiratory admissions: results from APHEA 2 project. Air Pollution and Health: a European Approach. Am J Respir Crit Care Med 164: 1860-1866.
24. Ling SH, van Eeden SF (2009) Particulate matter air pollution exposure: role in the development and exacerbation of chronic obstructive pulmonary disease. Int J Chron Obstruct Pulmon Dis 4: 233-243.
25. Stone V (2000) Environmental air pollution. Am J Respir Crit Care Med 162: S44-47.
26. Boezen M, Schouten J, Rijcken B, Vonk J, Gerritsen J, et al. (1998) Peak expiratory flow variability, bronchial responsiveness, and susceptibility to ambient air pollution in adults. Am J Respir Crit Care Med 158: 1848-1854.
27. Card JW, Zeldin DC, Bonner JC, Nestmann ER (2008) Pulmonary applications and toxicity of engineered nanoparticles. Am J Physiol Lung Cell Mol Physiol 295: L400-411.
28. Johnston HJ, Hutchison GR, Christensen FM, Peters S, Hankin S, et al. (2009) Identification of the mechanisms that drive the toxicity of TiO(2)particulates: the contribution of physicochemical characteristics. Part Fibre Toxicol 6: 33.
29. Ahn MH, Kang CM, Park CS, Park SJ, Rhim T, et al. (2005) Titanium dioxide particle-induced goblet cell hyperplasia: association with mast cells and IL-13. Respir Res 6: 34.
30. Garabrant DH, Fine LJ, Oliver C, Bernstein L, Peters JM (1987) Abnormalities of pulmonary function and pleural disease among titanium metal production workers. Scand J Work Environ Health 13: 47-51.
31. Chen HW, Su SF, Chien CT, Lin WH, Yu SL, et al. (2006) Titanium dioxide nanoparticles induce emphysema-like lung injury in mice. FASEB J 20: 2393-2395.
32. Hyun JS, Lee BS, Ryu HY, Sung JH, Chung KH, et al. (2008) Effects of repeated silver nanoparticles exposure on the histological structure and mucins of nasal respiratory mucosa in rats. Toxicol Lett 182: 24-28.
33. Voynow JA, Rubin BK (2009) Mucins, mucus, and sputum. Chest 135: 505-512.
34. Rogers DF (2007) Physiology of airway mucus secretion and pathophysiology of hypersecretion. Respir Care 52: 1134-1146; discussion 1146-1139.
35. Berridge MJ, Bootman MD, Roderick HL (2003) Calcium signalling: dynamics, homeostasis and remodelling. Nat Rev Mol Cell Biol 4: 517-529.
36. Ashby MC, Craske M, Park MK, Gerasimenko OV, Burgoyne RD, et al. (2002) Localized Ca2+ uncaging reveals polarized distribution of Ca2+-sensitive Ca2+ release sites: mechanism of unidirectional Ca2+ waves. J Cell Biol 158: 283-292.
37. Meissner G (1994) Ryanodine receptor/Ca2+ release channels and their regulation by endogenous effectors. Annu Rev Physiol 56: 485-508.
38. Solovyova N, Veselovsky N, Toescu EC, Verkhratsky A (2002) Ca(2+) dynamics in the lumen of the endoplasmic reticulum in sensory neurons: direct visualization of

Ca(2+)-induced Ca(2+) release triggered by physiological Ca(2+) entry. Embo J 21: 622-630.
39. Mogami H, Zhang H, Suzuki Y, Urano T, Saito N, et al. (2003) Decoding of short-lived Ca2+ influx signals into long term substrate phosphorylation through activation of two distinct classes of protein kinase C. J Biol Chem 278: 9896-9904.
40. Zhu H, Hille B, Xu T (2002) Sensitization of regulated exocytosis by protein kinase C. Proc Natl Acad Sci U S A 99: 17055-17059.
41. Brown DM, Donaldson K, Borm PJ, Schins RP, Dehnhardt M, et al. (2004) Calcium and ROS-mediated activation of transcription factors and TNF-alpha cytokine gene expression in macrophages exposed to ultrafine particles. Am J Physiol Lung Cell Mol Physiol 286: L344-353.
42. Brown DM, Hutchison L, Donaldson K, Stone V (2007) The effects of PM10 particles and oxidative stress on macrophages and lung epithelial cells: modulating effects of calcium-signaling antagonists. Am J Physiol Lung Cell Mol Physiol 292: L1444-1451.
43. Huang CC, Aronstam RS, Chen DR, Huang YW (2009) Oxidative stress, calcium homeostasis, and altered gene expression in human lung epithelial cells exposed to ZnO nanoparticles. Toxicol In Vitro 24: 45-55.
44. Stone V, Tuinman M, Vamvakopoulos JE, Shaw J, Brown D, et al. (2000) Increased calcium influx in a monocytic cell line on exposure to ultrafine carbon black. Eur Respir J 15: 297-303.
45. Dahiya R, Kwak KS, Byrd JC, Ho S, Yoon WH, et al. (1993) Mucin synthesis and secretion in various human epithelial cancer cell lines that express the MUC-1 mucin gene. Cancer Res 53: 1437-1443.
46. Chen E, Ruvalcaba M, Araujo L, Chapman R, Chin WC (2008) Ultrafine titanium dioxide nanoparticles induce cell death in human bronchial epithelial cells. Journal of Experimental Nanoscience 3: 171-183.
47. Gurr JR, Wang AS, Chen CH, Jan KY (2005) Ultrafine titanium dioxide particles in the absence of photoactivation can induce oxidative damage to human bronchial epithelial cells. Toxicology 213: 66-73.
48. Nguyen T, Chin WC, O'Brien JA, Verdugo P, Berger AJ (2001) Intracellular pathways regulating ciliary beating of rat brain ependymal cells. J Physiol 531: 131-140.
49. Kawasaki S, Takizawa H, Takami K, Desaki M, Okazaki H, et al. (2001) Benzene-extracted components are important for the major activity of diesel exhaust particles: effect on interleukin-8 gene expression in human bronchial epithelial cells. Am J Respir Cell Mol Biol 24: 419-426.
50. Edwards DA, Prausnitz MR, Langer R, Weaver JC (1995) Analysis of Enhanced Transdermal Transport by Skin Electroporation. Journal of Controlled Release 34: 211-221.
51. Kemp PA, Sugar RA, Jackson AD (2004) Nucleotide-mediated mucin secretion from differentiated human bronchial epithelial cells. Am J Respir Cell Mol Biol 31: 446-455.
52. Stone V, Johnston H, Clift MJ (2007) Air pollution, ultrafine and nanoparticle toxicology: cellular and molecular interactions. IEEE Trans Nanobioscience 6: 331-340.

53. Barlow PG, Clouter-Baker A, Donaldson K, Maccallum J, Stone V (2005) Carbon black nanoparticles induce type II epithelial cells to release chemotaxins for alveolar macrophages. Part Fibre Toxicol 2: 11.
54. Sayes CM, Wahi R, Kurian PA, Liu Y, West JL, et al. (2006) Correlating nanoscale titania structure with toxicity: a cytotoxicity and inflammatory response study with human dermal fibroblasts and human lung epithelial cells. Toxicol Sci 92: 174-185.
55. Zhang AP, Sun YP (2004) Photocatalytic killing effect of TiO2 nanoparticles on Ls-174-t human colon carcinoma cells. World J Gastroenterol 10: 3191-3193.
56. Petersen CC, Toescu EC, Petersen OH (1991) Different patterns of receptor-activated cytoplasmic Ca2+ oscillations in single pancreatic acinar cells: dependence on receptor type, agonist concentration and intracellular Ca2+ buffering. Embo J 10: 527-533.
57. Donaldson K, Stone V, Borm PJ, Jimenez LA, Gilmour PS, et al. (2003) Oxidative stress and calcium signaling in the adverse effects of environmental particles (PM10). Free Radic Biol Med 34: 1369-1382.
58. Berridge MJ, Irvine RF (1984) Inositol trisphosphate, a novel second messenger in cellular signal transduction. Nature 312: 315-321.
59. Berridge MJ, Irvine RF (1989) Inositol phosphates and cell signalling. Nature 341: 197-205.
60. Brown DM, Hutchison L, Donaldson K, MacKenzie SJ, Dick CA, et al. (2007) The effect of oxidative stress on macrophages and lung epithelial cells: the role of phosphodiesterases 1 and 4. Toxicol Lett 168: 1-6.
61. Boulton CL, O'Shaughnessy CT (1991) The Effect of Calcium Channel Antagonists on Spontaneous and Evoked Epileptiform Activity in the Rat Neocortex In Vitro. Eur J Neurosci 3: 992-1000.
62. Kelly CV, Leroueil PR, Orr BG, Banaszak Holl MM, Andricioaei I (2008) Poly(amidoamine) dendrimers on lipid bilayers II: Effects of bilayer phase and dendrimer termination. J Phys Chem B 112: 9346-9353.
63. Chou HT, Wen HW, Kuo TY, Lin CC, Chen WJ (2010) Interaction of cationic antimicrobial peptides with phospholipid vesicles and their antibacterial activity. Peptides 31: 1811-1820.
64. Gelis C, Girard S, Mavon A, Delverdier M, Paillous N, et al. (2003) Assessment of the skin photoprotective capacities of an organo-mineral broad-spectrum sunblock on two ex vivo skin models. Photodermatology Photoimmunology & Photomedicine 19: 242-253.
65. Levine KE, Fernando RA, Lang M, Essader A, Wong BA (2003) Development, and validation of a high-throughput method for the determination of titanium dioxide in rodent lung and lung-associated lymph node tissues. Analytical Letters 36: 563-576.
66. Lomer MCE, Thompson RPH, Powell JJ (2002) Fine and ultrafine particles of the diet: influence on the mucosal immune response and association with Crohn's disease. Proceedings of the Nutrition Society 61: 123-130.
67. Centi G, Ciambelli P, Perathoner S, Russo P (2002) Environmental catalysis: trends and outlook. Catalysis Today 75: 3-15.

68. Pirkanniemi K, Sillanpaa M (2002) Heterogeneous water phase catalysis as an environmental application: a review. Chemosphere 48: 1047-1060.
69. Wagner V, Dullaart A, Bock AK, Zweck A (2006) The emerging nanomedicine landscape. Nat Biotechnol 24: 1211-1217.
70. Pison U, Welte T, Giersig M, Groneberg DA (2006) Nanomedicine for respiratory diseases. Eur J Pharmacol 533: 341-350.
71. Truong-Le VL, Walsh SM, Schweibert E, Mao HQ, Guggino WB, et al. (1999) Gene transfer by DNA-gelatin nanospheres. Arch Biochem Biophys 361: 47-56.
72. Colvin VL (2003) The potential environmental impact of engineered nanomaterials. Nat Biotechnol 21: 1166-1170.
73. Byrne JD, Baugh JA (2008) The significance of nanoparticles in particle-induced pulmonary fibrosis. Mcgill J Med 11: 43-50.
74. Lkhasuren O, Takahashi K, Dash-Onolt L (2007) Occupational lung diseases and the mining industry in Mongolia. Int J Occup Environ Health 13: 195-201.
75. Mossman BT, Borm PJ, Castranova V, Costa DL, Donaldson K, et al. (2007) Mechanisms of action of inhaled fibers, particles and nanoparticles in lung and cardiovascular diseases. Part Fibre Toxicol 4: 4.
76. Xia T, Li N, Nel AE (2009) Potential Health Impact of Nanoparticles. Annu Rev Public Health 30: 137-150.
77. Lorimer WV, Lilis R, Fischbein A, Daum S, Anderson H, et al. (1978) Health Status of Styrene-Polystyrene Polymerization Workers. Scand J Work Environ Health 4: 220-226.
78. Quinton PM (2008) Cystic fibrosis: impaired bicarbonate secretion and mucoviscidosis. Lancet 372: 415-417.
79. Boucher RC (2007) Airway surface dehydration in cystic fibrosis: pathogenesis and therapy. Ann Rev Med 58: 157-170.
80. Donaldson SH, Bennett WD, Zeman KL, Knowles MR, Tarran R, et al. (2006) Mucus clearance and lung function in cystic fibrosis with hypertonic saline. N Engl J Med 354: 241-250.
81. Mall M, Grubb BR, Harkema JR, O'Neal WK, Boucher RC (2004) Increased airway epithelial Na+ absorption produces cystic fibrosis-like lung disease in mice. Nat Med 10: 487-493.
82. Klaine SJ, Alvarez PJJ, Batley GE, Fernandes TF, Handy RD, et al. (2008) Nanomaterials in the environment: Behavior, fate, bioavailability, and effects. Environ Toxicol Chem 27: 1825-1851.
83. Berger JT, Voynow JA, Peters KW, Rose MC (1999) Respiratory carcinoma cell lines. MUC genes and glycoconjugates. Am J Respir Cell Mol Biol 20: 500-510.
84. Chin WC, Orellana MV, Verdugo P (1998) Spontaneous assembly of marine dissolved organic matter into polymer gels. Nature 391: 568-572.
85. Espinosa M, Noe G, Troncoso C, Ho SB, Villalon M (2002) Acidic pH and increasing [Ca(2+)] reduce the swelling of mucins in primary cultures of human cervical cells. Hum Reprod 17: 1964-1972.
86. Tanaka T, Fillmore D (1979) Kinetics of swelling of gels. J Chem Phys 70: 1214-1218.

87. Bhaskar KR, Gong D, Bansil R, Pajevic S, Hamilton JA, et al. (1991) Profound Increase in Viscosity and Aggregation of Pig Gastric Mucin at Low Ph. Am J Physiol 261: G827-G833.
88. Verdugo P, Tam PY, Butler J (1983) Conformational structure of respiratory mucus studied by laser correlation spectroscopy. Biorheology 20: 223-230.
89. Edwards SF, Grant JWV (1973) Effect of Entanglements on Viscosity of a Polymer Melt. J Phys A: Math Gen 6: 1186-1195.
90. Edwards SF, Grant JWV (1973) Effect of Entanglements on Diffusion in a Polymer Melt. J Phys A: Math Gen 6: 1169-1185.
91. Lodge TP (1999) Reconciliation of the molecular weight dependence of diffusion and viscosity in entangled polymers. Phys Rev Lett 83: 3218-3221.
92. Satija J, Gupta U, Jain NK (2007) Pharmaceutical and biomedical potential of surface engineered dendrimers. Crit Rev Ther Drug Carrier Syst 24: 257-306.
93. Verdugo P, Aitken M, Langley L, Villalon MJ (1987) Molecular mechanism of product storage and release in mucin secretion. II. The role of extracellular Ca++. Biorheology 24: 625-633.
94. Rose MC (1992) Mucins: structure, function, and role in pulmonary diseases. Am J Physiol 263: L413-429.
95. Sheehan JK, Carlstedt I (1984) Hydrodynamic properties of human cervical-mucus glycoproteins in 6M-guanidinium chloride. Biochem J 217: 93-101.
96. Sheehan JK, Oates K, Carlstedt I (1986) Electron microscopy of cervical, gastric and bronchial mucus glycoproteins. Biochem J 239: 147-153.
97. Di Cola E, Yakubov GE, Waigh TA (2008) Double-globular structure of porcine stomach mucin: a small-angle X-ray scattering study. Biomacromolecules 9: 3216-3222.
98. Felgentreff K, Beisswenger C, Griese M, Gulder T, Bringmann G, et al. (2006) The antimicrobial peptide cathelicidin interacts with airway mucus. Peptides 27: 3100-3106.
99. Mayol L, Quaglia F, Borzacchiello A, Ambrosio L, La Rotonda MI (2008) A novel poloxamers/hyaluronic acid in situ forming hydrogel for drug delivery: rheological, mucoadhesive and in vitro release properties. Eur J Pharm Biopharm 70: 199-206.
100. Sandberg T, Blom H, Caldwell KD (2009) Potential use of mucins as biomaterial coatings. I. Fractionation, characterization, and model adsorption of bovine, porcine, and human mucins. J Biomed Mater Res A. pp. 762-772.
101. Sandberg T, Karlsson Ott M, Carlsson J, Feiler A, Caldwell KD (2009) Potential use of mucins as biomaterial coatings. II. Mucin coatings affect the conformation and neutrophil-activating properties of adsorbed host proteins--toward a mucosal mimic. J Biomed Mater Res A 91: 773-785.
102. Yakubov GE, Papagiannopoulos A, Rat E, Easton RL, Waigh TA (2007) Molecular structure and rheological properties of short-side-chain heavily glycosylated porcine stomach mucin. Biomacromolecules 8: 3467-3477.
103. Liu K, Ding HJ, Liu J, Chen Y, Zhao XZ (2006) Shape-controlled production of biodegradable calcium alginate gel microparticles using a novel microfluidic device. Langmuir 22: 9453-9457.

104. Lu L, Liu X, Tong Z, Gao Q (2006) Critical exponents and self-similarity for sol-gel transition in aqueous alginate systems induced by in situ release of calcium cations. J Phys Chem B 110: 25013-25020.
105. Cao X, Bansil R, Bhaskar KR, Turner BS, LaMont JT, et al. (1999) pH-dependent conformational change of gastric mucin leads to sol-gel transition. Biophys J 76: 1250-1258.
106. Lai SK, O'Hanlon DE, Harrold S, Man ST, Wang YY, et al. (2007) Rapid transport of large polymeric nanoparticles in fresh undiluted human mucus. Proc Natl Acad Sci U S A 104: 1482-1487.
107. Dawson M, Wirtz D, Hanes J (2003) Enhanced viscoelasticity of human cystic fibrotic sputum correlates with increasing microheterogeneity in particle transport. J Biol Chem 278: 50393-50401.
108. Kas HS (1997) Chitosan: properties, preparations and application to microparticulate systems. J Microencapsul 14: 689-711.
109. Song JS, Kang CM, Yoo MB, Kim SJ, Yoon HK, et al. (2007) Nitric oxide induces MUC5AC mucin in respiratory epithelial cells through PKC and ERK dependent pathways. Respir Res 8: 28.
110. Yuan-Chen Wu D, Wu R, Reddy SP, Lee YC, Chang MM (2007) Distinctive epidermal growth factor receptor/extracellular regulated kinase-independent and -dependent signaling pathways in the induction of airway mucin 5B and mucin 5AC expression by phorbol 12-myristate 13-acetate. Am J Pathol 170: 20-32.
111. Chin WC, Quesada I, Steed J, Verdugo P (2005) Modeling Ca-polyanion crosslinking in secretory networks. Assessment of charge density and bond affinity in polyanionic secretory networks. Macromol Symp 227: 89-96.
112. Tam PY, Verdugo P (1981) Control of mucus hydration as a Donnan equilibrium process. Nature 292: 340-342.
113. Quinton PM (2001) The neglected ion: HCO3. Nat Med 7: 292-293.
114. Bodian M (1953) Fibrocystic Disease of the Pancreas: A congenital disorder of mucus production -- mucosis. New York: Grune and Stratton,Inc. 1-244 p.
115. Oppenheimer EH, Esterly JR (1975) Pathology of cystic fibrosis review of the literature and comparison with 146 autopsied cases. Perspect Pediatr Pathol 2: 241-278.
116. Boucher RC (2007) Evidence for airway surface dehydration as the initiating event in CF airway disease. J Intern Med 261: 5-16.
117. Zabner J, Smith JJ, Karp PH, Widdicombe JH, Welsh MJ (1998) Loss of CFTR chloride channels alters salt absorption by cystic fibrosis airway epithelia in vitro. Mol Cell 2: 397-403.
118. Quinton PM (1999) Physiological basis of cystic fibrosis: a historical perspective. Physiol Rev 79: S3-S22.
119. Kuver R, Lee SP (2004) Calcium binding to biliary mucins is dependent on sodium ion concentration: relevance to cystic fibrosis. Biochem Biophys Res Commun 314: 330-334.
120. Kuver R, Wong T, Klinkspoor JH, Lee SP (2006) Absence of CFTR is associated with pleiotropic effects on mucins in mouse gallbladder epithelial cells. Am J Physiol Gastrointest Liver Physiol 291: G1148-1154.

121. Barasch J, Kiss B, Prince A, Saiman L, Gruenert D, et al. (1991) Defective acidification of intracellular organelles in cystic fibrosis. Nature 352: 70-73.
122. Forstner JF, Forstner GG (1975) Calcium binding to intestinal goblet cell mucin. Biochim Biophys Acta 386: 283-292.
123. Choi JY, Muallem D, Kiselyov K, Lee MG, Thomas PJ, et al. (2001) Aberrant CFTR-dependent HCO3- transport in mutations associated with cystic fibrosis. Nature 410: 94-97.
124. Quinton PM, editor (2001) HCO3- and Cystic Fibrosis. Genova: E.S. Burioni Ricerche Bibliografiche. 154 p.
125. Garcia MA, Yang N, Quinton PM (2009) Normal mouse intestinal mucus release requires cystic fibrosis transmembrane regulator-dependent bicarbonate secretion. J Clin Invest 119: 2613-2622.
126. Muchekehu RW, Quinton PM (2010) A new role for bicarbonate secretion in cervico-uterine mucus release. J Physiol 588: 2329-2342.
127. Harmon GS, Dumlao DS, Ng DT, Barrett KE, Dennis EA, et al. (2010) Pharmacological correction of a defect in PPAR-gamma signaling ameliorates disease severity in Cftr-deficient mice. Nat Med 16: 313-318.
128. Rubinstein M (1987) Discretized Model of Entangled-Polymer Dynamics. Phys Rev Lett 59: 1946-1949.
129. Schefer U, Ammann D, Pretsch E, Oesch U, Simon W (1986) Neutral Carrier Based Ca-2+-Selective Electrode with Detection Limit in the Sub-Nanomolar Range. Anal Chem 58: 2282-2285.
130. Baudet S, Hove-Madsen L, Bers DM (1994) How to make and use calcium-specific mini- and microelectrodes. Methods Cell Biol 40: 93-113.
131. Kreda SM, Okada SF, van Heusden CA, O'Neal W, Gabriel S, et al. (2007) Coordinated release of nucleotides and mucin from human airway epithelial Calu-3 cells. J Physiol 584: 245-259.
132. Jayaraman S, Song Y, Vetrivel L, Shankar L, Verkman AS (2001) Noninvasive in vivo fluorescence measurement of airway-surface liquid depth, salt concentration, and pH. J Clin Invest 107: 317-324.
133. Ishiguro H, Steward MC, Wilson RW, Case RM (1996) Bicarbonate secretion in interlobular ducts from guinea-pig pancreas. J Physiol 495 (Pt 1): 179-191.
134. Patnaik P (2002) Handbook of Inorganic Chemical Compounds McGraw-Hill handbooks: McGraw-Hill Professional, 2002. 1086 p.
135. Neuman WF, Morrow PE, Toribara TY, Casarett LJ, Mulryan BJ, et al. (1956) Evidence for Complex Ion Formation in the Calcium Bicarbonate System. J Biol Chem 219: 551-555.
136. Verdugo P (1984) Hydration kinetics of exocytosed mucins in cultured secretory cells of the rabbit trachea: a new model. Ciba Found Symp 109: 212-225.
137. Kesimer M, Makhov AM, Griffith JD, Verdugo P, Sheehan JK (2010) Unpacking a gel-forming mucin: a view of MUC5B organization after granular release. Am J Physiol Lung Cell Mol Physiol 298: L15-22.
138. Quinton PM (2010) Birth of mucus. Am J Physiol Lung Cell Mol Physiol 298: L13-14.
139. Garcia AB, Quinton P (2006) HCO3- Enhances Mucus Release In Mouse Small Intestine. . Pediatric Pulmonology Supplement 21